

1  
2  
3  
4  
5  
6  
7  
8  
9  
10  
11  
12  
13  
14  
15  
16  
17  
18  
19  
20  
21  
22  
23  
24  
25  
26  
27  
28  
29  
30  
31

## Accounting for cardiac t-tubule increase with age and myocyte volume to improve measurements of its membrane area and ionic current densities

Georges Christé<sup>1,2\*</sup>, Robert Bonvallet<sup>3</sup> and Christophe Chouabe<sup>4</sup>

<sup>1</sup> Laboratoire de Neurocardiologie, EA4612, Université Lyon 1, Lyon, F-69003, France

<sup>2</sup> INSERM, ADR Lyon, Lyon, F-69003 France

<sup>3</sup> CNRS UMR 5123, Campus de la Doua, Université Claude Bernard Lyon 1, 69622 Villeurbanne, France

<sup>4</sup> Université Lyon, CarMeN Laboratory, Institut National de la Santé et de la Recherche Médicale, Institut National de la Recherche Agronomique, Institut National des Sciences Appliquées de Lyon, Lyon, Université Claude Bernard Lyon 1, Bron, France

**Keywords:** cardiac myocytes, rat, t-tubule, volume, capacitance, morphology, weight, age, model

Declarations of interest: none.

\* Corresponding author:

Georges Christé, EA 4612 Neurocardiologie, Université Lyon1, Faculté de Pharmacie de Lyon, 8, avenue Rockefeller, 69373 Lyon Cedex 08, France

Email: [christe.georges@laposte.net](mailto:christe.georges@laposte.net)

Tél: +33 627556373

fax: +33 478777118

32  
33  
34  
35  
36  
37  
38  
39  
40  
41  
42  
43  
44  
45  
46  
47  
48  
49  
50  
51  
52

**Abstract**

*In-silico* models of cardiac myocytes allow simulating experiments in numbers on series of myocytes as well as on large populations of myocytes assembled in 3D structures. The simulated myocyte populations should have realistic values and statistical dispersions of biophysical parameters such as myocyte dimensions and volume and areas of the peripheral membrane and transverse-axial tubular system (TATS). Dependencies among these variables also have to be taken into account. In this work, we propose a quantitative representation of the changes in the fraction of membrane area in the TATS that integrates published dependencies with body weight (age) and size of rat ventricular cardiac myocytes while respecting the above constraints. Imposing a constant total membrane area-to-volume ratio appears to account for the increase of this fraction with myocyte size (i.e.: volume) within a given age group. The agreement of our results with published data was discussed and reasons for discrepancies were analysed. On the basis of our framework, strategies are proposed for minimising the influence of non-random dispersion related to myocyte volume on measurements of the area of TATS and surface membrane compartments and of ionic current densities. The next step will be to quantitatively compare these strategies by evaluating the impact of myocyte morphological parameters and their dependencies, sample size, biases and errors, on the output of experiments.

53 **Abbreviations**

54

55	AV-node	atrio-ventricular node
56	$C_m$	whole-cell membrane capacitance
57	di-8-ANEPPS	4-(2-[6-(Diocetyl-amino)-2-naphthalenyl]ethenyl)-1-(3-
58		sulfopropyl)pyridinium
59	$f_{\text{tres}}$	fraction of the TATS membrane that resisted detubulation
60	$l$	myocyte length
61	$l_{\text{mean}}$	average length
62	peri	perimeter of the cross-section of a myocyte
63	SA-node	sino-atrial node
64	$SD_l$	standard deviation of the length $l$
65	$SD_w$	standard deviation of the width $w$
66	$SD_{\text{th}}$	standard deviation of the thickness $th$
67	$S_{\text{end}}$	area of the end surface of a myocyte (~cross-sectional area)
68	$S_{\text{long}}$	area of the longitudinal surface of a myocyte
69	$S_{\text{surf}}$	area of the peripheral membrane of a myocyte
70	$S_{\text{tot}}$	total membrane area of a myocyte
71	$S_{\text{tt}}$	membrane surface area of the TATS in a myocyte
72	$th$	myocyte thickness
73	$th_{\text{mean}}$	average thickness
74	TATS	transverse-axial tubular system
75	$V_{\text{myo}}$	myocyte volume
76	$S_{\text{tot}}/V_{\text{myo}}$	ratio of total membrane area to myocyte volume
77	$S_{\text{tt}}/S_{\text{tot}}$	ratio of TATS membrane area to total membrane area
78	$S_{\text{tt}}/V_{\text{myo}}$	ratio of TATS membrane area to myocyte volume
79	$S_{\text{surf}}/V_{\text{myo}}$	ratio of surface membrane area to myocyte volume
80	$V_{\text{myo}}$	myocyte volume
81	$w$	myocyte width
82	$w_{\text{mean}}$	average width

83

84

## 85 **1 Introduction**

86

87 It has early been recognized that the amount of transverse-axial tubular system (TATS)  
88 increased with age (Page and McCallister, 1973a; Nakamura et al., 1986) and with myocyte  
89 size (Leeson, 1978; Satoh et al., 1996). It also was seen that ventricular myocytes have large  
90 amounts of TATS whereas atrial myocytes generally have a lower amount (Leeson, 1978;  
91 Leeson, 1980; Yue et al., 2017). In experimental rat models of cardiac hypertrophy (thyroid  
92 hormone), it was detected that myocytes have larger size and lower peripheral membrane area  
93 to myocyte volume ratio than in controls (McCallister and Page, 1973; Page and McCallister,  
94 1973b). However, their total membrane area to myocyte volume ratio was kept to control  
95 values, owing to the increase in the amount of TATS. The hypothesis was thus formulated  
96 that the purpose of the increase in TATS was to maintain a constant membrane area to  
97 myocyte volume ratio (McCallister and Page, 1973; Page and McCallister, 1973b). Owing to  
98 3D reconstruction in confocal microscopy of living myocytes using a membrane-bound  
99 fluorescent marker, this idea was confirmed by the demonstration that the total membrane  
100 area increases in linear relation to myocyte volume (Satoh et al., 1996; Swift et al., 2006) in  
101 control rats. Indeed, the membrane area to myocyte volume ratio is a characteristic for a given  
102 species at a particular age (or body weight) and is maintained across differences in size of  
103 ventricular myocytes at that age (Satoh et al., 1996). In the present work, we simulate these  
104 changes and extend this simulation to younger ages (i.e.: lower body weights) to test whether  
105 the constraint of a constant area to volume ratio might reproduce the increase in the amount of  
106 TATS reported during development. Care was taken to incorporate the most detailed  
107 descriptions of the shape of ventricular myocytes. In particular, documented quantitative  
108 relationships among length, width and thickness of myocytes were taken into account, as well  
109 as the contribution of membrane infolding and caveolae and the most plausible estimate of the  
110 specific membrane capacitance value. Conflicting values in published accounts of the  
111 quantitative importance of TATS in ventricular cardiac myocytes of rats have been discussed  
112 (Soeller and Cannell, 1999; Pasek et al., 2008b). We review these papers critically and  
113 explore whether such differences might have been due to measurement artefacts and/or to  
114 using animals of different ages, hence of different body weights.

115

116

## 117 **2 Methods**

118

### 119 *2.1 Softwares*

120 All computations used in this work were written as scripts suited to both Matlab (The  
121 MathWorks, Natick, MA, USA) and Scilab (ESI Group, Rungis, France) further data  
122 processing and figures were prepared under Origin 7 (OriginLab Corporation, Northampton,  
123 MA, USA).

124

### 125 *2.2 Rationale for building a synthetic set of data to represent changes in TATS with age or* 126 *weight and myocyte size.*

127 The morphological model to represent a cardiac ventricular myocyte was chosen to be a rod  
128 with ellipsoid cross section. A synthetic data set was generated: several sizes were chosen to  
129 span the 95% confidence interval of width, length and depth as measured by (Satoh et al.,  
130 1996). This was done for the two age groups i.e. 3 months (~350 g body weight) and 6  
131 months (~500 g body weight) studied by Satoh et al. (1996), as described in the Appendix.  
132 Two additional data sets were generated by extrapolating myocyte sizes down to rat weights  
133 of 250 and 200 g (corresponding to younger rats). The two basic assumptions were that  
134 average myocyte size increased linearly with age (or body weight, see 4.5 Limitations), and  
135 that the relative dispersion of myocyte dimensions was the same as in the data of Satoh et al.  
136 (1996). In addition, a volume rendering factor was applied to convert the computed volume to  
137 rendered myocyte volume (Satoh et al., 1996).

138 The peripheral area and volume were computed for each myocyte size of the synthetic data set  
139 as indicated above and in the Appendix.

140 The peripheral area to volume ratio was computed. The whole-myocyte capacitance to  
141 volume ratio was set to the values reported by Satoh et al. i.e.: 6.76 pF/pL for 3 months (~350  
142 g) and 8.88 pF/pL for 6 months (~500 g) rats, and we assumed that the total capacitance to  
143 volume ratio at 3 months would also apply when extending our simulations to younger  
144 animals (250 and 200 g). Under the hypothesis that the extent of TATS membrane area would  
145 ensure that the total membrane area to volume ratio is maintained, the expected value of the  
146 fraction of membrane in the TATS was computed from those data.

147 Several corrections were applied to take into account the presence of peripheral membrane  
148 grooves, caveolae and of infolding of the membrane at the intercalated disk, which all

149 increase the membrane area. Instead of the consensual value of  $1 \mu\text{F}/\text{cm}^2$ , a more realistic  
150 value of  $0.9 \mu\text{F}/\text{cm}^2$  was used to translate membrane capacitance into area (see Appendix).

151

### 152 **3 Results**

153

#### 154 *3.1 A constrained design for artificial series of myocytes*

155

#### 156 **Figure 1 near here**

157

158 We started with the assumptions that the myocytes were elongated rods with elliptic cross  
159 section and that myocyte width and thickness were linearly related to myocyte length. We  
160 created artificial datasets with lengths spanning the confidence interval around the mean  
161 length from published measurements for two average animal weights: 350 g (3 months) and  
162 500 g (6 months). This was extrapolated down to two smaller average animal weights. We  
163 then computed the area of the peripheral myocyte membrane including corrections for  
164 membrane infolding, caveolae and intercalated disks. We also computed the myocyte volume  
165 and applied a volume-rendering factor proper to each average animal weight to adjust for  
166 indentations of the myocytes. The peripheral membrane area to myocyte volume ratio was  
167 then derived. Fig. 1A shows that it increases when myocyte volume decreases. The shape of  
168 the relationship is quite similar at all rat ages. This increase is a non-linear function of  
169 myocyte volume and shows a steeper increase at smaller volumes. The maximal value of the  
170 peripheral membrane area to myocyte volume ratio is at the smallest volume for the younger  
171 rat age (diamonds for the 200 g series in Fig. 1A) and amounts to  $0.46 \mu\text{m}^2/\mu\text{m}^3$ . A similar  
172 relationship was established for Sprague-Dawley rats  $S_{\text{surf}}/V_{\text{myo}}$  ratio decreasing from  $0.53$   
173  $\mu\text{m}^2/\mu\text{m}^3$  for 44.5 g body weight down to about  $0.30 \mu\text{m}^2/\mu\text{m}^3$  at 300 g (Stewart and Page  
174 1978). We also plotted the relations of myocyte volume to projected area (length \* width) in  
175 Fig. 1B, showing that volume increases slightly more than projected area in all synthetic data  
176 series. However when statistical errors would be added, the relation might be treated as linear  
177 as done in figure 4A of Satoh et al. (1996).

178 Knowing  $S_{\text{surf}}/V_{\text{myo}}$  and  $S_{\text{tot}}/V_{\text{myo}}$ , the ratio  $S_{\text{tt}}/V_{\text{myo}}$  was derived for each myocyte size in each  
179 series corresponding to different animal weights (or age). It was computed as the difference  
180 from  $S_{\text{surf}}/V_{\text{myo}}$  to the constrained  $S_{\text{tot}}/V_{\text{myo}}$ . Then,  $S_{\text{tt}}/S_{\text{tot}}$  was computed by dividing  $S_{\text{tt}}/V_{\text{myo}}$   
181 by  $S_{\text{tot}}/V_{\text{myo}}$  (see in Appendix). As verification, whole myocyte  $C_m$  values were computed  
182 from the sum of  $S_{\text{surf}}$  and  $S_{\text{tt}}$  after conversion using a specific capacitance of  $0.9 \mu\text{F}/\text{cm}^2$ . Fig.

183 1C shows that our datasets respect the initial assumption of a constant  $C_m$  to  $V_{myo}$  ratio within  
184 a given age group.

185

186

**Figure 2 near here**

187

188 The  $S_{tt}/S_{tot}$  data of all series are displayed in Fig. 2 (open symbols with line) versus myocyte  
189 volume and show that the values of  $S_{tt}/S_{tot}$  vary considerably with myocyte size within each  
190 age group, but also between groups with the age of the animals, and that this fraction  
191 increases steeply with myocyte size when starting from the smaller myocyte sizes. The  
192 increase with myocyte volume is relatively small at later ages.

193 These graphs are duplicated in Fig. 2A and Fig. 2B and serve as a basis for comparing our  
194 simulation with values of the TATS membrane fraction that were derived from morphological  
195 studies, see 3.3 below.

196

197

198 *3.2 Are published morphological estimates of the fraction of membrane in TATS in conflict?*

199 The original data reported in various studies using morphological methods in electron  
200 microscopy or confocal microscopy have been collected in Tab. 1, and used to compute  
201 values of  $S_{tt}/S_{tot}$ , after applying corrections as explained in the Appendix.

202 We had to adjust our computations to the particular conditions of each study, which is  
203 detailed here below.

204

205

**Table 1 near here**

206

207 *3.2.1 Satoh et al. (1996):* The peripheral membrane area for an ellipsoid cross section  
208 myocyte having average dimensions as in table 2 of Satoh et al. was computed. Additionally,  
209 we took into account corrections for caveolae, membrane infolding and intercalated disk  
210 membrane folding. We also computed the myocyte volumes from myocyte dimensions in  
211 Satoh et al.'s work, and, in order to match the average rendered volumes that they evaluated  
212 by 3D analysis for 3 months and 6 months rats, the rendering factor that we had to apply was  
213 0.74 and 0.73 respectively. The values of  $S_{surf}/V_{myo}$ , computed from these estimates are  $0.308$   
214  $\mu\text{m}^2/\mu\text{m}^3$  for the 3 months rat and  $0.295 \mu\text{m}^2/\mu\text{m}^3$  for the 6 months rat. This yields values of  
215  $S_{tt}/S_{tot}$  of 0.544 and 0.668 respectively. The  $C_m/V_{myo}$  values of 6.76 and 8.88 pF/pL for 3 and  
216 6 months respectively, were converted into  $S_{tot}/V_{myo}$  of  $0.676 \mu\text{m}^2/\mu\text{m}^3$  and  $0.888 \mu\text{m}^2/\mu\text{m}^3$

217 using a specific capacitance of  $1 \mu\text{F}/\text{cm}^2$ . When a specific capacitance value of  $0.9 \mu\text{F}/\text{cm}^2$   
218 was used,  $S_{\text{tt}}/S_{\text{tot}}$  was computed to 0.589 and 0.702 for 3 months and 6 months rats  
219 respectively.

220

221 3.2.2 *Soeller and Cannell (1999)*: They report a single  $S_{\text{tt}}/V_{\text{myo}}$  value of  $0.44 \mu\text{m}^2/\mu\text{m}^3$ . This  
222 value is the largest estimate of  $S_{\text{tt}}/V_{\text{myo}}$  (Tab. 1). Using a hypothetical myocyte of cylindrical  
223 shape  $100 \mu\text{m}$  by  $20 \mu\text{m}$ , and the resulting volume of  $31400 \mu\text{m}^3$ , they estimated the ratio  
224  $S_{\text{tot}}/V_{\text{myo}}$  to  $6.6 \mu\text{m}^2/\mu\text{m}^3$ , a value near to that reported by Satoh et al. (1996) for 3 months  
225 Sprague-Dawley rats weighting 350 g. Assuming a specific capacitance of  $1 \mu\text{F}/\text{cm}^2$  they  
226 estimated the  $S_{\text{tt}}/V_{\text{myo}}$  to 0.68. This was when assuming  $S_{\text{tot}}/V_{\text{myo}}$  at  $0.676 \mu\text{m}^2/\mu\text{m}^3$ , as for 350  
227 g male Sprague-Dawley rats. Assuming in turn the ratio  $S_{\text{tot}}/V_{\text{myo}}$  to be 0.843 or 0.76  
228  $\mu\text{m}^2/\mu\text{m}^3$ , as derived from Swift et al. (2007) and Swift et al. (2006) respectively, for 300 g  
229 male Wistar rats, would yield an  $S_{\text{tt}}/S_{\text{tot}}$  value of 0.52 or 0.58. Soeller and Cannell (1999) used  
230 250 g male Wistar rats, thus the  $S_{\text{tt}}/S_{\text{tot}}$  of 0.52 may be considered as a lower limit and the  
231 value of 0.58 as an upper limit. These values changed to 0.47 and 0.52 respectively when  
232 considering a specific capacitance of  $0.9 \mu\text{F}/\text{cm}^2$ . It is surprising that Soeller and Cannell did  
233 not estimate  $S_{\text{surf}}$  and  $V_{\text{myo}}$ , which would have readily allowed estimation of  $S_{\text{tt}}/S_{\text{tot}}$ .

234

235 3.2.3 *Swift et al. (2006)* A ratio of mean myocyte  $C_m$  to mean  $V_{\text{myo}}$  of  $8.43 \text{ pF}/\text{pL}$  was  
236 computed from their data. Assuming a specific capacitance of  $0.9 \mu\text{F}/\text{cm}^2$ , this is converted to  
237 a  $S_{\text{tot}}/V_{\text{myo}}$  of  $0.94 \mu\text{m}^2/\mu\text{m}^3$ . The  $S_{\text{surf}}/V_{\text{myo}}$  computed from the data in Satoh et al. (1996) for a  
238 myocyte of 200 pF capacitance (the mean value reported in Swift et al. (2006)) with an  
239 elliptical cross section amounts to  $0.361 \mu\text{m}^2/\mu\text{m}^3$ . Thus the  $S_{\text{tt}}/S_{\text{tot}}$  may be estimated to 0.62.  
240 It would be 0.57 with a specific capacitance of  $1 \mu\text{F}/\text{cm}^2$ .

241

242 3.2.4 *Page et al. (1971)* The authors reported, in 200 g Sprague-Dawley rats, an  $S_{\text{surf}}/V_{\text{myo}}$  of  
243  $0.27 \mu\text{m}^2/\mu\text{m}^3$  and a  $S_{\text{tot}}/V_{\text{myo}}$  of  $0.34 \mu\text{m}^2/\mu\text{m}^3$ . A direct calculation leads to an estimated  
244  $S_{\text{tt}}/S_{\text{tot}}$  of 0.207. Assuming that peripheral membrane infolding was duly taken into account in  
245 the stereological measurements and that caveolae were likely neglected, both ratios should be  
246 corrected for the presence of caveolae. In this case, as we assumed the caveolae to increase  
247 membrane area by the same factor in peripheral and in TATS membrane, such correction  
248 would not change the computed  $S_{\text{tt}}/S_{\text{tot}}$ .

249



250 3.2.5 *Pager (1971)* Jeanne Pager used 200 g Wistar rats. The reported value of  $0.25 \mu\text{m}^2/\mu\text{m}^3$   
251 for  $S_{\text{tt}}/V_{\text{myo}}$  may be combined with an estimated  $S_{\text{tot}}/V_{\text{myo}}$  of  $0.44 \mu\text{m}^2/\mu\text{m}^3$ , as evaluated by  
252 Swift et al. (2006) in 300 g male Wistar rats. In this case the  $S_{\text{tt}}/S_{\text{tot}}$  would be 0.57. If now  
253 using a value of  $0.9 \text{ pF}/\text{cm}^2$  and in addition, correcting  $S_{\text{tt}}$  for caveolae, a value of 0.61 is  
254 computed. Lastly, using a  $S_{\text{tot}}/V_{\text{myo}}$  of  $0.76 \mu\text{m}^2/\mu\text{m}^3$  (computed assuming a specific  
255 capacitance of  $1 \mu\text{F}/\text{cm}^2$  from Swift et al.'s (2007)  $C_{\text{m}}/V_{\text{myo}}$  estimate of  $7.6 \text{ pF}/\text{pL}$ ) and  
256 correcting  $S_{\text{tt}}$  for caveolae a new value of  $S_{\text{tt}}/S_{\text{tot}}$  of 0.39 is estimated, that is changed to 0.35  
257 when considering  $0.9 \mu\text{F}/\text{cm}^2$ .

258

259 3.2.6 *Page and McCallister (1973a)* From their measurements of  $0.30 \mu\text{m}^2/\mu\text{m}^3$  and  $0.39$   
260  $\mu\text{m}^2/\mu\text{m}^3$  for respectively  $S_{\text{surf}}/V_{\text{myo}}$  and  $S_{\text{tot}}/V_{\text{myo}}$ , the  $S_{\text{tt}}/S_{\text{tot}}$  may be estimated to 0.23. As for  
261 the data of Page et al. (1971), correcting for caveolae would not alter the final computed  
262  $S_{\text{tt}}/S_{\text{tot}}$ .

263

264 3.2.7 *Page and Surdyk-Droske (1979)*: Their estimates of  $0.307 \mu\text{m}^2/\mu\text{m}^3$  for  $S_{\text{surf}}/V_{\text{myo}}$  and  
265  $0.145 \mu\text{m}^2/\mu\text{m}^3$  for  $S_{\text{tt}}/V_{\text{myo}}$  allow computing  $0.457 \mu\text{m}^2/\mu\text{m}^3$  for  $S_{\text{tot}}/V_{\text{myo}}$  and 0.32 for  $S_{\text{tt}}/S_{\text{tot}}$ .  
266 As was done above for the data of Page et al. (1971) and Page and McCallister (1973a), it  
267 may be assumed that infolding of the peripheral membrane has been taken into account, so  
268 that correcting  $S_{\text{surf}}/V_{\text{myo}}$  and  $S_{\text{tt}}/V_{\text{myo}}$  for caveolae did not change the  $S_{\text{tt}}/S_{\text{tot}}$  that remained to  
269 0.32.

270

271 3.2.8 *Nakamura et al. (1986)*: The same reasoning was applied to computations from the data  
272 of Nakamura et al. as from those of Pager (1971). The final estimates of  $S_{\text{tt}}/S_{\text{tot}}$  were 0.44 and  
273 0.48 for a specific capacitance at 1 and  $0.9 \mu\text{F}/\text{cm}^2$  respectively.

274

275 3.2.9 *Gorelik et al. (2006)*: They used fluorescence intensity measurements of the membrane  
276 probe di-8-ANEPPS on isolated living rat cardiomyocytes and computed the ratio of  
277 fluorescence intensity in a confocal slice of a myocyte, excluding the peripheral membrane, to  
278 the total fluorescence intensity within the same slice. Although they designated this ratio the  
279 "volume ratio" of the TATS, it may be taken to represent the ratio of  $S_{\text{tt}}/S_{\text{tot}}$ . However, this is  
280 valid under the assumption that the density of di-8-ANEPPS labelling per unit of membrane  
281 area was uniform over peripheral and TATS membrane compartments. The average "volume  
282 ratio" derived by Gorelik et al. was 0.728 for control myocytes, which is the highest estimate  
283 either published or computed on the basis of the present study. This ratio dropped to an

284 average of 0.432 after detubulation. Assuming that  $S_{\text{surf}}$  did not change, we computed that  
285 34% of the initial  $S_{\text{tt}}$  would remain after detubulation. See section 4.4 for further discussion.

286

### 287 *3.3 Comparison of estimates from morphological measurements to simulated values*

288 When the weight of the animals was given, we plotted the values of the  $S_{\text{tt}}/S_{\text{tot}}$  fraction as  
289 derived in section 3.2 (Tab. 1) versus the myocyte volume of the central point of the artificial  
290 data series that corresponded to their weight class. These appear in Fig. 2 as grey-filled  
291 symbols of the same type as the series corresponding to the rat weight reported by the authors.  
292 For convenience, these data have been overshadowed in grey colour in Tab.1 and numbers  
293 from the first column of Tab. 1 were added near the symbols in Fig. 2. The values for  
294 Sprague-Dawley rats appear in Fig. 2A. The large open symbols number 9 and 10 correspond  
295 to the study of Satoh et al. (1996). Our simulations overestimated the corresponding  $S_{\text{tt}}/S_{\text{tot}}$   
296 values of Tab. 1. This might be due to some inadequacy of the shape of a rod with elliptic  
297 cross-section that we chose. Although our computations were adjusted to correctly estimate  
298 the rendered volumes evaluated by Satoh et al. (1996), they may have underestimated the  
299 surface area of the myocytes. Our corrections for membrane infolding, caveolae and  
300 intercalated disk complexity may also need to be adjusted. Among studies on 200 g rats,  
301 studies (1), (4), (5) and (7) on Sprague-Dawley rats and (3), unidentified strain from Page and  
302 McCallister (1973a), are in reasonable match with our simulations. It should be noted that  
303 Page and co-workers, in studies (1), (5), (6) and (7) used Sprague-Dawley rats, which may  
304 apply for study (3). Study (12), on ~300 g rats, shows value sizeably lower than our  
305 simulation for 250 g rats. Study (6) on 300 g rats falls well below our simulations for 250 g  
306 (open triangles) or ~350 g rats (open squares). Study (14) is consistent with the highest weight  
307 class (open circles) of ~496 g rats and with study (10). As a whole, our simulations might be  
308 revised to better account for values from the literature on Sprague-Dawley rats, namely  
309 studies 9 and 10, which we took as a basis. In panel B of Fig. 2, we plotted the  $S_{\text{tt}}/S_{\text{tot}}$  values  
310 from Wistar rats. The upper value from study (2) and the value from study (8), for 200 g rats,  
311 are much higher than our simulation (open diamonds). The lower value from study (2) may be  
312 considered as consistent, as would both values from study (11) for 250 g rats. Study (13) is  
313 consistent with our simulation for ~350 g rats but was done on 300 g rats.

314 As a whole, the  $S_{\text{tt}}/S_{\text{tot}}$  values from morphological studies on both rat strains confirm a trend  
315 to increase with myocyte volume, as related to increasing body weight.

316

317

**Figure 3 near here**

318

319 *3.4 Comparing estimates of the TATS membrane fraction using morphological analysis versus*  
320 *C<sub>m</sub> analysis with formamide detubulation*

321 In order to compare all studies of Tab. 1 and 2, we gathered the data on two graphs in Fig. 3.  
322 Comparing the estimates from morphological studies (Tab. 1  $S_{ti}/S_{tot}$  values converted in %)   
323 with those based on formamide detubulation (Tab. 2), Fig. 3A shows a general  
324 underestimation by the latter, that holds when considering either Sprague-Dawley rats  
325 (lozenges) or Wistar rats (circles), whereas values for unidentified rat strains (triangles) are  
326 similar. For all studies specifying the weight of the rats, the  $S_{ti}/S_{tot}$  data from Tab. 1 were  
327 plotted in % versus weight in Fig. 3B. Data from studies that did not specify body weight  
328 were plotted on the left vertical axis. The data from detubulation studies in Wistar rats (open  
329 circles in Fig. 3B) include 9 data points within 250-300 g weights and two data points at 460  
330 g. The outlying data from Gadeberg et al. (2016) showing a TATS membrane fraction of  
331 14.2% ought to be disregarded, since it is more than two times lower than the value resulting  
332 from a parallel study (Bryant et al., 2015) on the same animals (see Tab. 2). The dispersion of  
333 the 10 remaining data points precludes any global visual relationship. Eight data points from  
334 morphological studies on Sprague-Dawley rats seem to indicate a positive correlation of  
335 TATS membrane fraction with weight. This is further analysed in section 4.3.

336

337

338 **Table 2 near here**

339

340 From the 20 reported measurements of loss of capacitance upon formamide detubulation of  
341 all studies on rat ventricular myocytes (Tab. 2), an average value of 28.5 % is computed for  
342 the TATS membrane fraction. Taking into account that, on average, detubulated myocytes  
343 still have about 8% of their TATS area remaining connected to the outside (Pasek et al.,  
344 2008a), or up to 16% (Bryant et al., 2015), we attempted to correct for the effect of a  $f_{tres}$   
345 value at 0.16 and computed values "% C<sub>m</sub> lost corr." in Tab. 2. We omitted the outlying value  
346 from Gadeberg et al. (2016), see above. The average corrected value of TATS membrane  
347 fraction of the remaining studies is at 35.7%. It is at 35.3% when considering only male  
348 Wistar rats. This would still be in the lower range of values from morphological studies at  
349 comparable body weights. Taking into account an average myocyte C<sub>m</sub> of 143 pF and a  
350 C<sub>m</sub>/V<sub>myo</sub> of 5.4 pF/pL (for 300 g rats), V<sub>myo</sub> ought to be 26.5 pL (Fig. 1C, open triangles). The  
351 TATS membrane fraction value corresponding to this volume in our simulation in Fig. 2 for a

352 300 g rat is 0.53. Thus, the TATS membrane fraction estimated from detubulation, even after  
353 correcting for incomplete detubulation, is sizeably lower than the expected values from our  
354 simulations and from morphological measurements (Tab. 1).

355

356

## 357 **4 Discussion**

358

### 359 *4.1 Myocyte dimensions and shape*

360 For their computations of myocyte volume, Boyett et al. (1991) used a rod with an elliptical  
361 cross section with a 1/3 ratio of width to thickness (Sorenson et al., 1985). The data in table 1  
362 of Satoh et al. (1996) for rat myocytes show a ratio at  $2.41 \pm 0.65$  (we estimated the error of  
363 0.65 after summing relative errors in width and depth). From table 2 of Satoh et al. (1996) we  
364 computed width to thickness ratios of 2.63 in adolescent rats and 2.42 in adult rats. In our  
365 simulated data sets, we generated a set of values with the same relative 95% confidence  
366 interval as the data of Satoh et al. in 6 months rats. It turns out that the width to thickness ratio  
367 varies between 2 and 2.7, the lower values being for smaller myocytes. This is consistent with  
368 the observation that myocytes from smaller animals tend to be less flattened (Sorenson et al.,  
369 1985). It appears that we chose the upper limit in setting the width to thickness to 3.0. In  
370 further simulations, we ought to adjust this parameter to a consensual value at 2.5 and  
371 possibly make it depend on myocyte length or age.

372 As to the length to width (l/w) ratio, the present synthetic data sets have l/w ratios spanning  
373 3.4 to 5.7 and showing a decrease when myocyte size increases. The following l/w values  
374 may be computed from published data in rat ventricular myocytes: 4.5 in rats of either sex  
375 250-300 g (Boyett et al., 1991); 5.03 in adult male Sprague-Dawley rats 250-350 g (Stimers  
376 and Dobretsov, 1998); 3.5 in female adult Wistar rats (Kawai et al., 1999); 5.02 in male  
377 Wistar rats (Brette et al., 2000); 3.85 in control and 3.08 in hypertrophied right ventricular  
378 myocytes from adult male Sprague-Dawley rats of 350-400 g (Chouabe et al., 1997); from  
379 3.76 to 4.54 in control (380-495 g) and 2.78 to 3.81 in hypertrophied myocytes from adult  
380 male Sprague-Dawley rats, with differences according to region in the left ventricle (Benitah  
381 et al., 1993). At change, Satoh et al. (1996) measured averaged length to width ratios of 4.19  
382 and 3.7 in 6 months (~500 g) and 3 months (~350 g) rats respectively. Thus the span of l/w  
383 ratios in our synthetic data set is consistent with ratios computed from published values and  
384 their changes along rat weight. Also of note, myocyte dimensions and l/w ratios did not differ  
385 among three rat strains at 3 months age, spontaneously hypertensive (SHR), Wistar-Kyoto

386 (WKY) and Fischer-344 rats, managed and studied in the same laboratory (Bishop et al.,  
387 1979), so we did not seek to explain discrepancies as resulting from morphological  
388 differences between rat strains.

389

#### 390 *4.2 The lower size limit for TATS morphogenesis*

391 Using electron microscopy, a lower limit of 7-8  $\mu\text{m}$  in myocyte diameter has been measured  
392 for rat ventricular myocytes to have a TATS (Hirakow, 1970). In living rat atrial myocytes  
393 under confocal microscopy, this limit appears between 11.7 and 13.2  $\mu\text{m}$  (Kirk et al., 2003).  
394 These two ranges of values come into agreement when considering a 45% myocyte shrinkage  
395 upon preparation for electron microscopy (Eisenberg and Mobley, 1975). In the present  
396 simulations, the peripheral membrane area to myocyte volume ratio increased when the size  
397 of a rod shape with elliptic cross section was decreased (Fig. 1A), so that, for a myocyte width  
398 of 12.9  $\mu\text{m}$ , the upper limit of the whole membrane area to volume ratio of  $6.76 \mu\text{m}^2/\mu\text{m}^3$  in  
399 3-months-rats was attained. Under the assumption that the amount of TATS is governed by  
400 this constraint, there would be no need for a 12  $\mu\text{m}$  wide myocyte of developing a TATS in  
401 the present synthetic data series. Thus the hypothesis of a constraint for a minimal membrane  
402 area to volume ratio could be enough to explain that the smaller atrial myocytes and yet  
403 smaller myocytes in the AV-node and SA-node are devoid of TATS (Brette et al., 2002).  
404 However, myocytes from very young rats having myocyte diameters as low as 7.8  $\mu\text{m}$  may  
405 still have a  $S_{\text{tt}}/S_{\text{tot}}$  of 13% (Stewart and Page 1978), pointing to a different determinism of the  
406 TATS in ventricular versus atrial or nodal cells.

407

#### 408 *4.3 Dependence of $S_{\text{tt}}/S_{\text{tot}}$ on rat weight*

409 The data generated in this study also account for the progressive increase in the amount of  
410 TATS as is evidenced in the EM micrographs of Nakamura et al. (1986) taken from the  
411 ventricle of 28 g up to 490-560 g Wistar rats in 7 different classes of weights and in the data  
412 of Stewart and Page (1978) for Sprague-Dawley rats 44.5 to 300 g body weight, yielding  
413 TATS membrane fractions increasing from 13% to about 35% respectively. Furthermore, the  
414 apparently high membrane fraction in TATS derived from the analysis of Soeller and Cannell  
415 (1999) for 250 g Wistar rats turns out to be in agreement with the data of Satoh et al. (1996)  
416 and with our simulation (Fig. 2B, study (11)) once plausible corrections were applied. The  
417 large value derived by Gorelik et al. (2006) by computing the ratio of TATS-related  
418 fluorescence to total fluorescence in a confocal slice is likely an overestimate, as discussed in  
419 4.4.

420

421

**Figure 4 near here**

422

423 It appeared in Fig. 2A that TATS membrane fraction data from morphological studies in  
424 Sprague-Dawley rats (filled lozenges) might indicate a correlation with body weight. A linear  
425 regression analysis is depicted in Fig. 4. Despite considering a reasonable 20% relative  
426 standard deviation in both TATS membrane fraction and weight data, a tight correlation was  
427 found. The fitted line intercept value at  $-10.4 \pm 17.5 \%$  cannot be considered as different from  
428 zero. The slope was estimated at  $0.167 \pm 0.065 \%/g$  with a low relative error. Thus, TATS  
429 membrane fraction may be considered as increasing proportionally to body weight. Of note,  
430 the TATS membrane fraction values read along the fitted line are 23% at 200 g and 31% at  
431 250 g body weight whereas in our simulations (Fig. 2) they are 26% and 46% respectively.  
432 Values at 346 and 496 g are 48% and 72.6% respectively versus 63% and 73% respectively in  
433 our simulation. This confirms that our simulations need adjustment to match the experimental  
434 data. Regarding data from Wistar rats in Fig. 3B, no such correlation was attempted from  
435 morphological data, since only 4 values are available and two of them are in contradiction.  
436 From detubulation studies, the outlier point from Gadeberg et al. (2006) being excluded, a  
437 single point remains outside of a cluster of points spanning a narrow weight range (250-300  
438 g). This is not surprising, because detubulation studies aimed at deriving data on the  
439 distribution of ion channels in standard conditions and mostly used young adults.

440

441 *4.4 Comparability of morphological and detubulation estimates of  $S_{tt}/S_{tot}$*

442

443 Overestimation of  $S_{tt}/S_{tot}$  might result from a slow internalisation of di-8-ANEPPS with time  
444 into the sarcoplasm (Chaloupka et al., 1997) unduly counted as tubular membrane  
445 fluorescence. However, this possibility was ruled out by Soeller and Cannell (1999). Another  
446 possible bias could arise if a single confocal slice was analysed in each myocyte and would be  
447 at the mid-height of a myocyte lying flat. Referring to the transverse sections shown in figure  
448 6 of Soeller and Cannell (1999) one may observe that this would maximize the volume of the  
449 slice and thereby the amount of TATS. In addition, the density of the TATS is maximal at  
450 mid-height. This would also minimize the area of peripheral membrane since most of the  
451 surface membrane will be oriented perpendicular to the plane of the confocal slice. In  
452 comparison, in a confocal slice nearing the upper or lower boundaries of the myocyte, the  
453 surface membrane plane will be obliquely oriented and will contribute a larger part of the

454 fluorescence signal, whereas the density of the TATS will be lower. The integrative 3D  
455 analyses of Satoh et al. (1996) and of Soeller and Cannell (1999) take all of the internal  
456 voxels into account, which avoids such drawbacks.

457 Thomas et al. (2003) reported complete detubulation while most other studies have evaluated  
458 a fraction of TATS resisting detubulation (non-detubulated and incompletely detubulated  
459 myocytes) from 8% (Pasek et al., 2008a) to 16% (Bryant et al. (2015) whereas we evaluated a  
460 high value at 36% from Gorelik et al.'s (2006) data. There could be an opportunity to improve  
461 the efficiency of formamide detubulation if the reasons of the full detubulation by Thomas et  
462 al. were deciphered. A possible explanation for a fraction of intact t-tubules remaining could  
463 be a partial protection of the TATS by small permeant molecules (Uchida et al., 2016).

464 When comparing the formamide detubulation procedure with that induced by imipramine,  
465 Bourcier et al. (2019) reported a decay of 45% of rod-shaped myocytes in male Wistar rats'  
466 ventricular myocytes upon formamide detubulation. If this decay would preferentially affect  
467 larger cells, the remaining myocytes would have lower TATS membrane fraction values,  
468 which might explain why Thomas et al. (2003) observed a low-range average TATS  
469 membrane fraction at 26.5% although all of their rod-shaped myocytes, after formamide  
470 treatment, appeared completely detubulated. Further, Bourcier et al. (2019) evaluated a TATS  
471 membrane fraction of 40% comparing imipramine-detubulated myocytes to control ones. This  
472 value is only at the higher range found from formamide-detubulation studies. Thus,  
473 inconvenients of the formamide detubulation revealed by the imipramine method did not  
474 resolve the discrepancy with morphological methods. Correcting the ensemble of data from  
475 detubulation studies for incomplete detubulation did not succeed either (see 3.4). This  
476 suggests that morphological studies did overestimate the TATS membrane fraction. One  
477 possible reason analysed by Pasek et al. (2008a) was the possibility that the specific  
478 capacitance of the TATS membrane might be lower than that of the surface membrane, due to  
479 a higher content in cholesterol. However, a recent study by Gadeberg et al. (2017) did not  
480 reveal a change in  $C_m/V_{myo}$  of mouse ventricular myocytes upon cholesterol depletion using  
481 methyl- $\beta$ -cyclodextrin. This does not preclude another unknown reason for the specific  
482 membrane capacitance to be different in surface and tubular membranes.

483

#### 484 4.5 *Limitations*

485 In this study, we referred to body weight and/or age of the animals, which may be confusing.  
486 The authors had preferred to be able to refer to one single parameter, i.e.: weight, because a  
487 larger body weight imposes an increased workload to the heart, causing physiological

488 hypertrophy at any age. Likewise, animal strain and gender are important parameters, and we  
489 did not attempt to consider possible differences. However, it readily appears from Tab. 1 that  
490 among 14 studies, eight of them omitted to specify either age (8) or body weight (1) or both  
491 (1). This also goes for omitting gender (4) or rat strain (2), and one study reported using male  
492 and female rats. Similarly, in Tab. 2, over 18 studies, age is omitted in 12 of them, body-  
493 weight in 7 and gender in 8. As a whole, methods have been under documented, which  
494 hinders attempts to figure out the influence of some parameters and provides sense to the  
495 "Minimum Information about a Cardiac Electrophysiology Experiment (MICCE)" initiative  
496 (Quinn et al. 2011). Whenever willing to translate from age to weight, we might refer to the  
497 values of ages and weights reported by Nakamura et al. (1986) for Wistar rats as plotted in  
498 Fig. 5. They show a proportional relationship from 1 week to 6 months with an increment of  
499 about 30 g/week. The data from Wistar rats (open circles) below 500 g agree well with  
500 Nakamura's data. The data from Sprague-Dawley rats of Satoh et al. (1996) at 3 months (~350  
501 g) agree with that relationship, as do those of Despa et al. (2003) and Garcarena et al. (2013)  
502 at 300 g. Data for ages around 6 months (25-27 weeks) from Wistar or Sprague-Dawley rats  
503 depart from the linear relation. Other studies in Tab. 2 reported age or weight or none, and the  
504 term "adult Wistar" was used for rats having weights ranging 250-300 g with two exceptions  
505 at 450 and 460 g.

506

507

### **Figure 5 near here**

508

509 In generating our datasets, it was assumed that myocyte width and depth changed in parallel  
510 to myocyte length and that the statistical dispersion of values in these three dimensions was  
511 principally due to differences in myocyte length. However, it was reported that the individual  
512 length to width ratio of ventricular myocytes of the rabbit ranged from 2.16 to 7.4 (Taniguchi  
513 et al., 1981). This suggests that there is a large independent variation of length and width of  
514 the myocytes, and that shorter myocytes do not necessarily have smaller widths. In this  
515 respect, the span of myocyte volumes in our synthetic data series may be exaggerated.  
516 It was shown that ventricular myocytes from adult rats appeared binucleated for 85% of them  
517 and 15% mononucleated. The mean length and width were significantly larger in binucleated  
518 myocytes and the volume was doubled, versus mononucleated ones (Bishop et al., 1979). This  
519 was neglected by Satoh et al. (1996) and may contribute to increase the dispersion around the  
520 mean dimensions of the myocytes. Thus, accounting for two separate populations should be



521 more accurate, not only for simulating, but perhaps also for analysing data from a population  
522 of rat ventricular myocytes.

523 An assumption in extrapolating to rats of lower weight classes (200 and 250 g) was that  
524 average myocyte dimensions would increase linearly with animal weight and that relative  
525 dispersion would remain constant. This is in agreement with a linear increase of myocyte  
526 length with body weight in Sprague-Dawley rats from 45 to 200 g of  $\sim 20 \mu\text{m/g}$  (Stewart and  
527 Page 1978).

528 It was assumed that the amount of TATS would ensure a constant area to volume ratio,  
529 however, the amount of TATS differs along the long axis of the myocyte, as it is larger at mid  
530 length of the myocyte than at its ends (Mitcheson et al., 1996; Quinn et al., 2003). Thus the  
531 amount of TATS may rather be correlated with local width as shown in mouse atrial  
532 myocytes (Yue et al., 2017).

533 Our assumption of a direct proportionality of  $C_m$  to  $V_{\text{myo}}$  within one class of weights cannot  
534 be directly supported by figure 4B of Satoh et al. (1996) because they analysed the relation of  
535  $V_{\text{myo}}$  to  $C_m$ . However, we have read data out from figure 4B of Satoh et al. and performed a  
536 linear regression of  $C_m$  to  $V_{\text{myo}}$  resulting in the relation:  $C_m = (7.5 \pm 1.4) * V_{\text{myo}} + (33 \pm 51)$   
537 (not shown). The large value of the error on the intercept at  $V_{\text{myo}}=0$  suggests that  $C_m$  is not  
538 different from zero at this point. Given the low relative error on the slope, we may assume  
539 that  $C_m$  was proportional to  $V_{\text{myo}}$ .

540

#### 541 *4.6 Determinants of TATS development*

542 Two functional requirements are in line with a constant area to volume ratio. The need to  
543 synchronize Ca release and hence contraction requires conduction of the excitation  
544 instantaneously to the whole myocyte volume, a function which is ensured by the voltage  
545 homogeneity of cardiac TATS membrane beyond microseconds after a voltage change, as  
546 evaluated in computer models of rat and guinea-pig ventricular myocytes (Pasek et al., 2006;  
547 Pasek et al., 2008b; Pasek et al., 2008c), in agreement with subcellular voltage sensitive dye  
548 measurements (Windisch et al., 1995; Sacconi et al. 2012), which was also confirmed by  
549 Scardigli et al. (2017) using FRAP microscopy. Furthermore, couplings of the membrane with  
550 the SR (dyads) ought to be present at short distance from the contractile material, to avoid  
551 diffusion delay from the periphery to contractile units, this would require extension of the  
552 TATS to the centre of the myocyte. Metabolic supply in states of high demand requires  
553 transfer of glucose to the myocyte interior. GLUT4 transporters are translocated both at  
554 peripheral and at TATS membranes under stimulation by insulin alone (Rett et al., 1996) or

555 associated with exercise (Slot et al., 1991). Therefore, the maximal glucose transfer rate to the  
556 myocyte ought to be proportional to the total membrane area. This shall also be true for ion  
557 transfer by mechanisms that are more evenly distributed, especially for the Na-K pump or the  
558 Na-Ca exchanger that regulate intracellular ion homeostasis. Molecular mechanisms that  
559 trigger and regulate the morphogenesis of TATS and its association with ion channels,  
560 receptors and effectors are being progressively deciphered as reviewed e.g.: by Ibrahim et al.  
561 (2011) and Hong and Shaw (2017).

562

#### 563 *4.7 Proper statistical distributions of biophysical parameters of cardiac myocytes*

564 The values of measurements done on single cardiac myocytes such as morphological and  
565 electrical parameters are generally assumed to be pseudo-Gaussian, so that computations of  
566 average, standard deviation and standard error on the mean use the canonical formulas of  
567 Gaussian statistics. However, almost all of these parameters are strictly positive quantities that  
568 may even have a sizeable minimal plausible value. These features apply to measured values of  
569 the capacitance of isolated rat ventricular cardiac myocytes. The Gaussian distribution, when  
570 the ratio of SD to mean is small, is deemed an acceptable approximation allowing statistical  
571 comparisons of experimental data series. However, when using Monte-Carlo simulations,  
572 creating artificial data series as Gaussian random numbers, we noted that unrealistic small (or  
573 even negative) values appeared, which compromised the statistical behaviour of the whole  
574 series. The Log-Gaussian distribution ensures that no values at or lower than zero can be  
575 generated, further, it behaves as Gaussian if the logarithm of the variable is considered, thus  
576 still allowing usual statistical comparisons (Limpert et al., 2001; Limpert and Stahel, 2011).

577

#### 578 *4.8 Statistical errors and their propagation in TATS membrane fraction determination*

579 In most studies using detubulation to evaluate TATS membrane fraction, two sub-populations  
580 are separated from a unique pool of isolated myocytes, one of which remains intact while the  
581 other is subjected to detubulation. Assuming perfect detubulation,  $C_m$  values are measured  
582 from a sample of  $n_i$  and  $n_d$  myocytes in each sub-population and the mean values ( $C_{mi}$  and  
583  $C_{md}$ ), each associated with its own standard deviation ( $sd_i$  and  $sd_d$ ) are used to compute the  
584 quantity  $a=(C_{mi}-C_{md})/C_{mi}$ . To evaluate the final standard deviation, absolute errors sum up for  
585 a subtraction and relative errors sum up for a division. Since  $C_{mi}-C_{md}$  will be at least 2 fold  
586 smaller than either  $C_{md}$  or  $C_{mi}$ , the final relative error on  $S_{ti}/S_{tot}$  is currently 3- to 4- fold larger  
587 than those of  $C_{mi}$  and  $C_{md}$  alone. When this further combines with ionic current values in  
588 order to evaluate current densities in surface and TATS membranes, average currents  $I_i$  in

589 intact myocytes and  $I_d$  in detubulated ones are combined to provide  $b=(I_i-I_d)/I_d$  the fraction of  
590 current in the TATS and  $b/a$  is then the current density in the TATS. When considering the  
591 mean values, if a large number of myocytes is studied, the central limit theorem tells us that  
592 the mean values will be well estimated, but the error will remain large and this will hinder  
593 conclusions about the statistical significance of the differences observed. An aggravating  
594 condition, as confirmed by the present study, is that a large part of the variability in  $C_m$  values  
595 is not due to random myocyte to myocyte variations, but  $C_{mi}$  depends on the size of the  
596 myocyte, and further, the TATS membrane fraction value does as well. One ideal way to  
597 circumvent these drawbacks would be to have each myocyte acting as its own control, and it  
598 is expected that the number of experiments to achieve a given level of significance of the  
599 differences might be affordable. It was proven possible to maintain a myocyte in conditions of  
600 whole-cell patch-clamp throughout the detubulation procedure (Kawai et al. 1999). This  
601 approach will require that the detubulation occurs soon enough to allow measurements being  
602 made before and after detubulation, and also that the measurement procedure be repeatable.  
603 For example, if imipramine-induced detubulation (Bourcier et al. 2019) is applicable in a few  
604 minutes and remains stable, it might be an alternative. Another possibility, within the separate  
605 populations of myocytes, would be to use myocytes of comparable size, thus eliminating the  
606 size-related variability, and for so doing, it might be preferable to pre-select myocytes having  
607 similar volumes, which can be evaluated with some precision using the projected area, since it  
608 was shown to be almost linearly related to myocyte volume (Satoh et al., 1996). In any case,  
609 such possibilities may well be simulated using our framework, once adjusted to closely  
610 represent the features of the myocytes from a given strain/species and a given age/weight  
611 class. This could help optimising a chosen strategy, or choosing among possible strategies to  
612 achieve a given goal in significance.

613

#### 614 *4.9 Applicability and relevance of our proposal*

615 The underlying assumption that the amount of TATS in a myocyte is increased so as to keep  
616 the myocyte membrane area to myocyte volume constant may apply to physiological rat  
617 hearts (Satoh et al., 1996), to myocyte hypertrophy due to thyroxin exposure (McCallister and  
618 Page, 1973; Page and McCallister, 1973a) or due to exercise in mouse hearts (Stolen et al.,  
619 2009) in which TATS density was kept constant while myocyte volume increased. However  
620 this does not necessarily apply to hypertrophy seen in pathological states where TATS may  
621 decrease or remain constant but changes shape or is disorganised (Seidel et al., 2017; Louch  
622 et al., 2010).

623 Our study has disclosed that the framework has to be adjusted to age/weight of the animals, to  
624 account for a particular set of myocytes. Application to the analysis of sets of myocytes from  
625 diseased regions of the myocardium might reveal a loss of inner linkages between biophysical  
626 parameters e.g.: TATS amount and myocyte size, suggesting that a regulatory mechanism is  
627 disrupted. Our approach may be applied to generate separate sets of cardiac myocytes with  
628 different inner linkages, which might perhaps help deciphering whether a mixture of two  
629 types of myocytes may account for an unaccountable apparent dispersion. It also could be  
630 used to generate subsets of myocytes corresponding to different regions, with different  
631 morphologies, electrophysiological properties or different inner TATS structures as in Colli-  
632 Franzone et al. (2006). Interestingly, a variable TATS distribution has recently been  
633 quantified in rat and pig atria as a decreasing transmural gradient from epicardium to  
634 endocardium, for which a role in synchronisation of contraction of the atrial wall was  
635 deciphered from mathematical modelling (Frisk et al., 2014). These authors also report three  
636 types of myocytes in rat atria: untubulated, tubulated and organized-tubulated while a single  
637 type of ventricular myocytes is found. A tight link of amplitude of the calcium current to  
638 myocyte capacitance and to  $C_m/V_{myo}$  is also revealed. The same group disclosed a difference  
639 in TATS amount between myocytes from the base and the apex in rat and mouse ventricles  
640 (Wright et al., 2018). Models of cardiac myocytes with different properties are generated to  
641 account for the behaviour of different populations of myocytes as to the state of their TATS,  
642 owing to heart failure (Loucks et al., 2018). These are approaches similar to ours in which  
643 once there are defined, for each subgroup, the myocyte parameters, the shape of their  
644 statistical distribution and the links between parameters, then realistic populations of  
645 myocytes can be generated and the behaviour of their combination into 3D tissue structures  
646 can be compared to that of uniform structures. Finally, our approach may well be combined  
647 with any detailed electro-ionic model of single myocytes, e.g.: (Livshitz et al., 2012), since  
648 only features at the whole myocyte level are generated in our approach.

649

## 650 **5 Conclusions:**

651 The proposed framework reasonably agrees with published data documenting the relations of  
652 TATS membrane fraction to myocyte volume within several classes of body weights. It  
653 provides a basis for analysing the sources of imprecision in the evaluation of the areas of  
654 TATS and surface membrane and their related ionic current densities. As a result, strategies  
655 are suggested for minimizing the influence of non-random data dispersion of TATS fraction  
656 related to myocyte volume. The framework described in this work might serve to generate

657 large sets of artificial isolated myocyte populations adapted to age and myocyte sizes, with  
658 realistic features, links between parameters and constrained statistical distributions. The next  
659 step is to use such datasets to evaluate the improvement of measurements depending on  
660 sample size, dependencies, biases and errors.

661

662

663 Reference List

664

665 Benitah, J.P., Gomez, A.M., Bailly, P., Da Ponte, J.P., Berson, G., Delgado, C., Lorente,  
666 P., 1993. Heterogeneity of the early outward current in ventricular cells isolated from normal  
667 and hypertrophied rat hearts. *J. Physiol.* 469, 111-138.

668 Bishop, S.P., Oparil, S., Reynolds, R.H., Drummond, J.L., 1979. Regional myocyte size  
669 in normotensive and spontaneously hypertensive rats. *Hypertension* 1, 378-383.

670 Bishop, S.P., Drummond, J.L., 1979. Surface morphology and cell size measurement of  
671 isolated rat cardiac myocytes. *J. Mol. Cell. Cardiol.* 11, 423-433.

672 Bourcier, A., Barthe, M., Bedioune, I., Lechene, P., Miled, H.B., Vandecasteele, G.,  
673 Fischmeister, R., Leroy, J., 2019. Imipramine as an alternative to formamide to detubulate rat  
674 ventricular cardiomyocytes. *Exp. Physiol.* 104, 1237-1249.

675 Boyett, M.R., Frampton, J.E., Kirby, M.S., 1991. The length, width and volume of  
676 isolated rat and ferret ventricular myocytes during twitch contractions and changes in osmotic  
677 strength. *Exp. Physiol.* 76, 259-270.

678 Brette, F., Calaghan, S.C., Lappin, S., White, E., Colyer, J., Le Guennec, J.Y., 2000.  
679 Biphasic effects of hypo-osmotic challenge on excitation- contraction coupling in rat  
680 ventricular myocytes. *Am. J. Physiol.* 279, H1963-H1971.

681 Brette, F., Komukai, K., Orchard, C.H., 2002. Validation of formamide as a  
682 detubulation agent in isolated rat cardiac cells. *Am. J. Physiol.* 283, H1720-H1728.

683 Brette, F., Salle, L., Orchard, C.H., 2004a. Differential modulation of L-type  $Ca^{2+}$   
684 current by SR  $Ca^{2+}$  release at the T-tubules and surface membrane of rat ventricular myocytes.  
685 *Circ. Res.* 95, e1-e7.

686 Brette, F., Rodriguez, P., Komukai, K., Colyer, J., Orchard, C.H., 2004b. Beta-  
687 adrenergic stimulation restores the Ca transient of ventricular myocytes lacking t-tubules. *J.*  
688 *Mol. Cell. Cardiol.* 36, 265-275.

689 Brette, F., Orchard, C.H., 2006a. Density and sub-cellular distribution of cardiac and  
690 neuronal sodium channel isoforms in rat ventricular myocytes. *Biochem. Biophys. Res.*  
691 *Commun.* 348, 1163-1166.

692 Brette, F., Orchard, C.H., 2006b. No apparent requirement for neuronal sodium  
693 channels in excitation-contraction coupling in rat ventricular myocytes. *Circ. Res.* 98, 667-  
694 674.

695 Bryant, S., Kimura, T.E., Kong, C.H., Watson, J.J., Chase, A., Suleiman, M.S., James,  
696 A.F., Orchard, C.H., 2014. Stimulation of ICa by basal PKA activity is facilitated by  
697 caveolin-3 in cardiac ventricular myocytes. *J. Mol. Cell Cardiol.* 68, 47-55.

698 Bryant, S.M., Kong, C.H., Watson, J., Cannell, M.B., James, A.F., Orchard, C.H., 2015.  
699 Altered distribution of ICa impairs Ca release at the t-tubules of ventricular myocytes from  
700 failing hearts. *J. Mol. Cell Cardiol.* 86, 23-31.

701 Chaloupka, R., Plasek, J., Slavik, J., Siglerova, V., Sigler, K., 1997. Measurement of  
702 membrane potential in *Saccharomyces cerevisiae* by the electrochromic probe di-4-ANEPPS:  
703 effect of intracellular probe distribution. *Folia Microbiol. (Praha).* 42, 451-456.

704 Chase, A., Colyer, J., Orchard, C.H., 2010. Localised Ca channel phosphorylation  
705 modulates the distribution of L-type Ca current in cardiac myocytes. *J. Mol. Cell. Cardiol.* 49,  
706 121-131.

707 Chouabe, C., Espinosa, L., Megas, P., Chakir, A., Rougier, O., Freminet, A., Bonvallet,  
708 R., 1997. Reduction of I(Ca,L) and I(to1) density in hypertrophied right ventricular cells by  
709 simulated high altitude in adult rats. *J. Mol. Cell. Cardiol.* 29, 193-206.

710 Colli-Franzone, P., Pavarino, L.F., Taccardi, B., 2006. Effects of transmural electrical  
711 heterogeneities and electrotonic interactions on the dispersion of cardiac repolarization and  
712 action potential duration: A simulation study. *Math. Biosci.* 204, 132-165.

713 Despa, S., Brette, F., Orchard, C.H., Bers, D.M., 2003. Na/Ca exchange and Na/K-  
714 ATPase function are equally concentrated in transverse tubules of rat ventricular myocytes.  
715 *Biophys. J.* 85, 3388-3396.

716 Despa, S., Bers, D.M., 2007. Functional analysis of Na<sup>+</sup>/K<sup>+</sup>-ATPase isoform  
717 distribution in rat ventricular myocytes. *Am. J. Physiol.* 293, C321-C327.

718 Ducholier, H., 2005. Neuronal sodium channels in ventricular heart cells are localized  
719 near T-tubules openings. *Biochem. Biophys. Res. Commun.* 334, 1135-1140.

720 Eisenberg, B.R., Mobley, B.A., 1975. Size changes in single muscle fibers during  
721 fixation and embedding. *Tissue Cell* 7, 383-387.

722 Frisk, M., Koivumaki, J.T., Norseng, P.A., Maleckar, M.M., Sejersted, O.M., Louch,  
723 W.E., 2014. Variable t-tubule organization and Ca<sup>2+</sup> homeostasis across the atria. *Am. J.*  
724 *Physiol. Heart Circ. Physiol.* 307, H609-H620.

725 Gadeberg, H.C., Bryant, S.M., James, A.F., Orchard, C.H., 2016. Altered Na/Ca  
726 exchange distribution in ventricular myocytes from failing hearts. *Am. J. Physiol. Heart Circ.*  
727 *Physiol.* 310, H262-H268.

728 Gadeberg, H.C., Kong, C.H.T., Bryant, S.M., James, A.F., Orchard, C.H., 2017.  
729 Cholesterol depletion does not alter the capacitance or Ca handling of the surface or t-tubule  
730 membranes in mouse ventricular myocytes. *Physiol. Rep.* 5, 5-22.

731 Garcarena, C.D., Ma, Y.L., Swietach, P., Huc, L., Vaughan-Jones, R.D., 2013.  
732 Sarcolemmal localisation of Na<sup>+</sup>/H<sup>+</sup> exchange and Na<sup>+</sup>-HCO<sub>3</sub><sup>-</sup> co-transport influences the  
733 spatial regulation of intracellular pH in rat ventricular myocytes. *J. Physiol.* 591, 2287-2306.

734 Gentet, L.J., Stuart, G.J., Clements, J.D., 2000. Direct measurement of specific  
735 membrane capacitance in neurons. *Biophys. J.* 79, 314-320.

736 Gilai, A., 1976. Electromechanical coupling in tubular muscle fibers. II. Resistance and  
737 capacitance of one transverse tubule. *J. Gen. Physiol.* 67, 343-367.

738 Gorelik, J., Yang, L.Q., Zhang, Y., Lab, M., Korchev, Y., Harding, S.E., 2006. A novel  
739 Z-groove index characterizing myocardial surface structure. *Cardiovasc. Res.* 72, 422-429.

740 Hirakow, R., 1970. Ultrastructural characteristics of the mammalian and sauropsidan  
741 heart. *Am. J. Cardiol.* 25, 195-203.

742 Hong, T.T., Shaw, R.M., 2017. Cardiac t-tubule microanatomy and function. *Physiol.*  
743 *Rev.* 97, 227-252.

744 Hoyt, R.H., Cohen, M.L., Saffitz, J.E., 1989. Distribution and three-dimensional  
745 structure of intercellular junctions in canine myocardium. *Circ. Res.* 64, 563-574.

746 Ibrahim, M., Gorelik, J., Yacoub, M.H., Terracciano, C.M., 2011. The structure and  
747 function of cardiac t-tubules in health and disease. *Proc. Biol. Sci.* 278, 2714-2723.

748 Kawai, M., Hussain, M., Orchard, C.H., 1999. Excitation-contraction coupling in rat  
749 ventricular myocytes after formamide-induced detubulation. *Am. Heart J.* 277, H603-H609.

750 Kirk, M.M., Izu, L.T., Chen-Izu, Y., McCulle, S.L., Wier, W.G., Balke, C.W.,  
751 Shorofsky, S.R., 2003. Role of the transverse-axial tubule system in generating calcium  
752 sparks and calcium transients in rat atrial myocytes. *J. Physiol.* 547.2, 441-451.

753 Komukai, K., Brette, F., Yamanushi, T.T., Orchard, C.H., 2002. K(+) current  
754 distribution in rat sub-epicardial ventricular myocytes. *Pflugers Arch.* 444, 532-538.

755 Leeson, T.S., 1978. The transverse tubular (T) system of rat cardiac muscle fibers as  
756 demonstrated by tannic acid mordanting. *Can. J. Zool.* 56, 1906-1916.

757 Leeson, T.S., 1980. T-tubules, couplings and myofibrillar arrangements in rat atrial  
758 myocardium. *Acta Anatomica* 108, 374-388.

759 Levin, K.R., Page, E., 1980. Quantitative studies on plasmalemmal folds and caveolae  
760 of rabbit ventricular myocardial cells. *Circ. Res.* 46, 244-255.



761 Lewis, C.J., Gong, H., Brown, M.J., Harding, S.E., 2004. Overexpression of beta 1-  
762 adrenoceptors in adult rat ventricular myocytes enhances CGP 12177A cardiostimulation:  
763 implications for 'putative' beta 4-adrenoceptor pharmacology. *Br. J Pharmacol.* 141, 813-824.

764 Limpert, E., Stahel, W.A., Abbt, M., 2001. Log-normal Distributions across the  
765 Sciences: Keys and Clues. *BioScience* 51, 341-352.

766 Limpert, E., Stahel, W.A., 2011. Problems with using the normal distribution--and ways  
767 to improve quality and efficiency of data analysis. *PLoS ONE* 6, e21403.

768 Livshitz, L., Acsai, K., Antoons, G., Sipido, K., Rudy, Y., 2012. Data-based theoretical  
769 identification of subcellular calcium compartments and estimation of calcium dynamics in  
770 cardiac myocytes. *J Physiol.* 590, 4423-4446.

771 Louch, W.E., Sejersted, O.M., Swift, F., 2010. There goes the neighborhood:  
772 pathological alterations in T-tubule morphology and consequences for cardiomyocyte Ca<sup>2+</sup>  
773 handling. *J. Biomed. Biotechnol.* 2010:503906. Epub 2010 Apr 8., 503906.

774 Loucks, A.D., O'Hara, T., Trayanova, N.A., 2018. Degradation of T-Tubular  
775 Microdomains and Altered cAMP Compartmentation Lead to Emergence of Arrhythmogenic  
776 Triggers in Heart Failure Myocytes: An in silico Study. *Front. Physiol.* 9:1737. doi:  
777 10.3389/fphys.2018.01737. eCollection@2018., 1737.

778 McCallister, L.P., Page, E., 1973. Effects of thyroxin on ultrastructure of rat myocardial  
779 cells: stereological study. *J. Ultrastruct. Res.* 42, 136-155.

780 Mitcheson, J.S., Hancox, J.C., Levi, A.J., 1996. Action potentials, ion channel currents  
781 and transverse tubule density in adult rabbit ventricular myocytes maintained for 6 days in  
782 cell culture. *Pflugers Arch.* 431, 814-827.

783 Nag, A.C., Fischman, D.A., Aumont, M.C., Zak, R., 1977. Studies of isolated adult rat  
784 heart cells: the surface morphology and the influence of extracellular calcium ion  
785 concentration on cellular viability. *Tissue Cell* 9, 419-436.

786 Nag, A.C., Zak, R., 1979. Dissociation of adult mammalian heart into single cell  
787 suspension: an ultrastructural study. *J. Anat.* 129, 541-559.

788 Nakamura, S., Asai, J., Hama, K., 1986. The transverse tubular system of rat  
789 myocardium: its morphology and morphometry in the developing and adult animal. *Anat.*  
790 *Embryol. (Berl.)* 173, 307-315.

791 Page, E., McCallister, L.P., Power, B., 1971. Stereological measurements of cardiac  
792 ultrastructures implicated in excitation-contraction coupling. *Proc. Natl. Acad. Sci. U. S. A.*  
793 68, 1465-1466.

794 Page, E., McCallister, L.P., 1973b. Studies on the intercalated disk of rat left ventricular  
795 myocardial cells. *J. Ultrastruct. Res.* 43, 388-411.

796 Page, E., McCallister, L.P., 1973a. Quantitative electron microscopic description of  
797 heart muscle cells: application to normal, hypertrophied and thyroxin treated hearts. *Am. J.*  
798 *Cardiol.* 31, 172-181.

799 Page, E., 1978. Quantitative ultrastructural analysis in cardiac membrane physiology.  
800 *Am. J. Physiol.* 235, C147-C158.

801 Page, E., Surdyk-Droske, M., 1979. Distribution, surface density, and membrane area of  
802 diadic junctional contacts between plasma membrane and terminal cisterns in mammalian  
803 ventricle. *Circ. Res.* 45, 260-267.

804 Pager, J., 1971. Etude morphométrique du système tubulaire transverse du myocarde  
805 ventriculaire de rat. *J. Cell Biol.* 50, 233-237.

806 Pasek, M., Simurda, J., Christé, G., 2006. The functional role of cardiac T-tubules  
807 explored in a model of rat ventricular myocytes. *Philos. Transact. A Math. Phys. Eng. Sci.*  
808 364, 1187-1206.

809 Pasek, M., Brette, F., Nelson, D.A., Pearce, C., Qaiser, A., Christé, G., Orchard, C.H.,  
810 2008a. Quantification of t-tubule area and protein distribution in rat cardiac ventricular  
811 myocytes. *Progress Biophys. Mol. Biol.* 96/1-3, 244-257.

812 Pasek, M., Simurda, J., Orchard, C.H., Christé, G., 2008b. A model of the guinea-pig  
813 ventricular cardiomyocyte incorporating a transverse-axial tubular system. *Prog. Biophys.*  
814 *Mol. Biol.* 96/1-3, 258-280.

815 Pasek, M., Simurda, J., Christé, G., Orchard, C.H., 2008c. Modelling the cardiac  
816 transverse-axial tubular system. *Progress Biophys. Mol. Biol.* 96/1-3, 226-243.

817 Pasek, M., Simurda, J., Christé, G., 2017. Different densities of Na-Ca exchange current  
818 in t-tubular and surface membranes and their impact on cellular activity in a model of rat  
819 ventricular cardiomyocyte. *Biomed Research International* 2017, 6343821.

820 Quinn, F.R., Currie, S., Duncan, A.M., Miller, S., Sayeed, R., Cobbe, S.M., Smith,  
821 G.L., 2003. Myocardial infarction causes increased expression but decreased activity of the  
822 myocardial Na<sup>+</sup>-Ca<sup>2+</sup> exchanger in the rabbit. *J. Physiol.* 553, 229-242.

823 Quinn, T.A., Granite, S., Alessie, M.A., Antzelevitch, C., Bollensdorff, C., Bub, G.,  
824 Burton, R.A., Cerbai, E., Chen, P.S., Delmar, M., DiFrancesco, D., Earm, Y.E., Efimov, I.R.,  
825 Egger, M., Entcheva, E., Fink, M., Fischmeister, R., Franz, M.R., Garny, A., Giles, W.R.,  
826 Hannes, T., Harding, S.E., Hunter, P.J., Iribe, G., Jalife, J., Johnson, C.R., Kass, R.S.,  
827 Kodama, I., Koren, G., Lord, P., Markhasin, V.S., Matsuoka, S., McCulloch, A.D., Mirams,

828 G.R., Morley, G.E., Nattel, S., Noble, D., Olesen, S.P., Panfilov, A.V., Trayanova, N.A.,  
829 Ravens, U., Richard, S., Rosenbaum, D.S., Rudy, Y., Sachs, F., Sachse, F.B., Saint, D.A.,  
830 Schotten, U., Solovyova, O., Taggart, P., Tung, L., Varro, A., Volders, P.G., Wang, K.,  
831 Weiss, J.N., Wettwer, E., White, E., Wilders, R., Winslow, R.L., Kohl, P., 2011. Minimum  
832 Information about a Cardiac Electrophysiology Experiment (MICEE): standardised reporting  
833 for model reproducibility, interoperability, and data sharing. *Prog. Biophys. Mol. Biol.* 107, 4-  
834 10.

835 Rett, K., Wicklmayr, M., Dietze, G.J., Haring, H.U., 1996. Insulin-induced glucose  
836 transporter (GLUT1 and GLUT4) translocation in cardiac muscle tissue is mimicked by  
837 bradykinin. *Diabetes* 45, S66-S69.

838 Sacconi, L., Ferrantini, C., Lotti, J., Coppini, R., Yan, P., Loew, L.M., Tesi, C., Cerbai,  
839 E., Poggesi, C., Pavone, F.S., 2012. Action potential propagation in transverse-axial tubular  
840 system is impaired in heart failure. *Proc. Natl. Acad. Sci. U. S. A.* 109, 5815-5819.

841 Satoh, H., Delbridge, L.M.D., Blatter, L.A., Bers, D.M., 1996. Surface:volume  
842 relationship in cardiac myocytes studied with confocal microscopy and membrane  
843 capacitance measurements: species-dependence and developmental effects. *Biophys. J.* 70,  
844 1494-1504.

845 Scardigli, M., Crocini, C., Ferrantini, C., Gabbrielli, T., Silvestri, L., Coppini, R., Tesi,  
846 C., Rog-Zielinska, E.A., Kohl, P., Cerbai, E., Poggesi, C., Pavone, F.S., Sacconi, L., 2017.  
847 Quantitative assessment of passive electrical properties of the cardiac T-tubular system by  
848 FRAP microscopy. *Proc. Natl. Acad. Sci. U. S. A.* 114, 5737-5742.

849 Seidel, T., Navankasattusas, S., Ahmad, A., Diakos, N.A., Xu, W.D., Tristani-Firouzi,  
850 M., Bonios, M.J., Taleb, I., Li, D.Y., Selzman, C.H., Drakos, S.G., Sachse, F.B., 2017. Sheet-  
851 Like Remodeling of the Transverse Tubular System in Human Heart Failure Impairs  
852 Excitation-Contraction Coupling and Functional Recovery by Mechanical Unloading.  
853 *Circulation.* 135, 1632-1645.

854 Severs, N.J., Slade, A.M., Powell, T., Twist, V.W., Warren, R.L., 1982. Correlation of  
855 ultrastructure and function in calcium-tolerant myocytes isolated from the adult rat heart. *J.*  
856 *Ultrastruct. Res.* 81, 222-239.

857 Severs, N.J., Slade, A.M., Powell, T., Twist, V.W., Jones, G.E., 1985. Morphometric  
858 analysis of the isolated calcium-tolerant cardiac myocyte. Organelle volumes, sarcomere  
859 length, plasma membrane surface folds, and intramembrane particle density and distribution.  
860 *Cell Tissue Res.* 240, 159-168.

861 Slot, J.W., Geuze, H.J., Gigengack, S., James, D.E., Lienhard, G.E., 1991.  
862 Translocation of the glucose transporter GLUT4 in cardiac myocytes of the rat. *Proc. Natl.*  
863 *Acad. Sci. U. S. A.* 88, 7815-7819.

864 Soeller, C., Cannell, M.B., 1999. Examination of the transverse tubular system in living  
865 cardiac rat myocytes by 2-photon microscopy and digital image-processing techniques. *Circ.*  
866 *Res.* 84, 266-275.

867 Sorenson, A.L., Tepper, D., Sonnenblick, E.H., Robinson, T.F., Capasso, J.M., 1985.  
868 Size and shape of enzymatically isolated ventricular myocytes from rat and cardiomyopathic  
869 hamsters. *Cardiovasc. Res.* 19, 793-799.

870 Stewart, J.M., Page, E., 1978. Improved stereological techniques for studying  
871 myocardial cell growth: application to external sarcolemma, T system, and intercalated disks  
872 of rabbit and rat hearts. *J. Ultrastruct. Res.* 65, 119-134.

873 Stimers, J.R., Dobretsov, M., 1998. Adrenergic stimulation of Na/K pump current in  
874 adult rat cardiac myocytes in short-term culture. *J. Membr. Biol.* 163, 205-216.

875 Stolen, T.O., Hoydal, M.A., Kemi, O.J., Catalucci, D., Ceci, M., Aasum, E., Larsen, T.,  
876 Rolim, N., Condorelli, G., Smith, G.L., Wisloff, U., 2009. Interval training normalizes  
877 cardiomyocyte function, diastolic Ca<sup>2+</sup> control, and SR Ca<sup>2+</sup> release synchronicity in a  
878 mouse model of diabetic cardiomyopathy. *Circ. Res.* 105, 527-536.

879 Swift, F., Stromme, T.A., Amundsen, B., Sejersted, O.M., Sjaastad, I., 2006. Slow  
880 diffusion of K<sup>+</sup> in the T tubules of rat cardiomyocytes. *J. Appl. Physiol.* 101, 1170-1176.

881 Swift, F., Tovsrud, N., Enger, U.H., Sjaastad, I., Sejersted, O.M., 2007. The Na<sup>+</sup>/K<sup>+</sup>-  
882 ATPase alpha2-isoform regulates cardiac contractility in rat cardiomyocytes. *Cardiovasc. Res.*  
883 75, 109-117.

884 Swift, F., Birkeland, J.A., Tovsrud, N., Enger, U.H., Aronsen, J.M., Louch, W.E.,  
885 Sjaastad, I., Sejersted, O.M., 2008. Altered Na<sup>+</sup>/Ca<sup>2+</sup>-exchanger activity due to  
886 downregulation of Na<sup>+</sup>/K<sup>+</sup>-ATPase alpha2-isoform in heart failure. *Cardiovasc. Res.* 78, 71-  
887 78.

888 Taniguchi, J., Kokubun, S., Noma, A., Irisawa, H., 1981. Spontaneously active cells  
889 isolated from the sino-atrial and atrio-ventricular nodes of the rabbit heart. *Jpn. J. Physiol.* 31,  
890 547-558.

891 Thomas, M.J., Sjaastad, I., Andersen, K., Helm, P.J., Wasserstrom, J.A., Sejersted,  
892 O.M., Ottersen, O.P., 2003. Localization and function of the Na<sup>+</sup>/Ca<sup>2+</sup> exchanger in normal  
893 and detubulated rat cardiomyocytes. *J. Mol. Cell. Cardiol.* 35, 1325-1337.

894 Uchida, K., Moench, I., Tamkus, G., Lopatin, A.N., 2016. Small membrane permeable  
895 molecules protect against osmotically induced sealing of t-tubules in mouse ventricular  
896 myocytes. *Am. J. Physiol. Heart Circ. Physiol.* 311, H229-H238.

897 Windisch, H., Ahammer, H., Schaffer, P., Muller, W., Platzer, D., 1995. Optical  
898 multisite monitoring of cell excitation phenomena in isolated cardiomyocytes. *Pflugers Arch.*  
899 430, 508-518.

900 Wright, P.T., Bhogal, N.K., Diakonov, I., Pannell, L.M.K., Perera, R.K., Bork, N.I.,  
901 Schobesberger, S., Lucarelli, C., Faggian, G., Alvarez-Laviada, A., Zaccolo, M., Kamp, T.J.,  
902 Balijepalli, R.C., Lyon, A.R., Harding, S.E., Nikolaev, V.O., Gorelik, J., 2018.  
903 Cardiomyocyte Membrane Structure and cAMP Compartmentation Produce Anatomical  
904 Variation in beta2AR-cAMP Responsiveness in Murine Hearts. *Cell Rep.* 23, 459-469.

905 Yang, Z., Pascarel, C., Steele, D.S., Komukai, K., Brette, F., Orchard, C.H., 2002. Na<sup>+</sup>-  
906 Ca<sup>2+</sup> exchange activity is localized in the T-tubules of rat ventricular myocytes. *Circ. Res.*  
907 91, 315-322.

908 Yao, A., Spitzer, K.W., Ito, N., Zaniboni, M., Lorell, B.H., Barry, W.H., 1997. The  
909 restriction of diffusion of cations at the external surface of cardiac myocytes varies between  
910 species. *Cell Calcium* 22, 431-438.

911 Yue, X., Zhang, R., Kim, B., Ma, A., Philipson, K.D., Goldhaber, J.I., 2017.  
912 Heterogeneity of transverse-axial tubule system in mouse atria: Remodeling in atrial-specific  
913 Na<sup>(+)</sup>-Ca<sup>(2+)</sup> exchanger knockout mice. *J. Mol. Cell Cardiol.* 108:50-60. doi:  
914 10.1016/j.yjmcc.2017.05.008. Epub@2017 May@19, 50-60.

915

916

## 917 6 Appendix

918

919 This section explains the bases for our computation and how we conducted them.

920

### 921 6.1 Myocyte dimensions

922 It is intuitive that the peripheral area to volume ratio of an object keeping constant shape shall  
923 decrease as its volume increases, since volume increases faster than peripheral area. However,  
924 to obtain a quantitative representation of this phenomenon in cardiac myocytes, a suitable  
925 morphological model has to be designed. Ventricular cardiac myocytes resemble rods with a  
926 rather short outfit. In vertical projection, their aspect is almost rectangular with partial  
927 spindle-like narrowing towards its ends and irregularities in width. Models used by various  
928 experimenters to estimate myocyte volume from the measured length and width (and  
929 sometimes depth) have differed in the shape of the cross section: rectangular (parallelepiped),  
930 circular (cylinder), ellipsoid with rectangular vertical projection or spindle-like with circular  
931 or ellipsoid cross-section. These models have been compared by Satoh et al. (Satoh et al.,  
932 1996) for the ability of the volumes (computed using measured length, width and depth) to  
933 account for 3D-rendered volume analysed from confocal imaging of freshly dissociated  
934 myocytes. The rendered volume was 0.54 times that of the parallelepiped, 1.42 times that of  
935 the spindle but 0.71 times that of the rod with ellipsoid cross section (Satoh et al., 1996). In  
936 the present development, the myocyte was assumed to have an elongated rod-like shape with  
937 ellipsoid cross section with a ratio of thickness to width of about 1/3 (Sorenson et al., 1985;  
938 Boyett et al., 1991). Myocyte dimensions were assumed to have negligible measurement error  
939 (an absolute error of  $\pm 0.5 \mu\text{m}$  seems an acceptable assumption). The cell-to-cell dispersion of  
940 length values around the mean was consensually reported by authors with mean  $\pm$  SD (or sem  
941 and n) as if it would follow a normal distribution. A series of equally spaced length values  
942 was generated, spanning the interval mean-SD to mean+SD. An odd number of values were  
943 generated, so that the mean value would be represented as the central value.

944 The ratio of myocyte length to myocyte width is preserved across myocyte sizes in rat left  
945 ventricular myocytes (Bishop and Drummond 1979). The ratio of myocyte thickness to  
946 myocyte width may be considered as constant (Sorenson et al., 1985; Boyett et al., 1991).  
947 Thus, myocyte width and thickness were assumed to be linear functions of myocyte length  
948 within ventricular myocytes from rats of a given weight and were computed so that their  
949 values span the mean-SD to mean+SD interval of measurements by Satoh et al. (1996).

950

951 The general formula was

$$952 \quad w = (l - l_{\text{mean}}) / SD_l * SD_w + w_{\text{mean}} \text{ (in } \mu\text{m)} \quad (\text{A1})$$

$$953 \quad th = (l - l_{\text{mean}}) / SD_l * SD_{th} + th_{\text{mean}} \text{ (in } \mu\text{m)} \quad (\text{A2})$$

954

955 thus, for 6 months rats:

$$956 \quad w = (l - 140.1) / 16.4 * 4.8 + 33.4 \text{ (in } \mu\text{m)} \text{ and} \quad (\text{A3})$$

$$957 \quad th = (l - 140.1) / 16.4 * 1.5 + 13.8 \text{ (in } \mu\text{m)}; \quad (\text{A4})$$

958

959 and for 3 months rats:

$$960 \quad w = (l - 123.8) / 14.4 * 6.7 + 33.6 \text{ (in } \mu\text{m)} \text{ and} \quad (\text{A5})$$

$$961 \quad th = (l - 123.8) / 14.4 * 1.4 + 12.8 \text{ (in } \mu\text{m)}. \quad (\text{A6})$$

962

963 The perimeter of the elliptic cross section was computed using an approximate formula:

$$964 \quad \text{peri} = \pi * \text{sqrt} [ 2 * (a^2+b^2) - (a-b)^2/2 ] \text{ with } a = w/2 \text{ and } b = th/2 \quad (\text{A7})$$

965 (<http://www.numericana/answer/ellipse.htm>) that has a relative precision of about  $4 * 10^{-13}$ .

$$966 \quad S_{\text{end}} = \pi * w * th / 4 \quad (\text{A8})$$

967 (in  $\mu\text{m}^2$ ) is the area of the intercalated disks at one end of the myocyte;

$$968 \quad S_{\text{long}} = \text{peri} * l \quad (\text{A9})$$

969 (in  $\mu\text{m}^2$ ) is the side area of the myocyte (excluding intercalated disks);

$$970 \quad S_{\text{surf}} = S_{\text{long}} + S_{\text{end}} * 2 \quad (\text{A10})$$

971 (in  $\mu\text{m}^2$ ) is the total myocyte surface area;

$$972 \quad V_{\text{myo}} = S_{\text{end}} * l \quad (\text{A11})$$

973 (in  $\mu\text{m}^3$ ) is the myocyte volume.

974

## 975 6.2 Extrapolation to lower rat weights

976 Myocyte length is in approximate linear relation with weight (Stewart and Page 1978) and the  
977 ratio of myocyte length to myocyte width is almost constant (Sorenson et al., 1985).

978 Therefore putative theoretical mean values of myocyte length ( $l_{\text{mean}}$ ), width ( $w_{\text{mean}}$ ) and  
979 thickness ( $th_{\text{mean}}$ ) were extrapolated from 6 months rat data (496 g) down to weights (W) of  
980 250 and 200 g, using:

981

$$982 \quad l_{\text{mean}} = (140.1-123.8) / (496-346) * (W-346) + 123.8 \quad (\text{A12})$$

983

$$984 \quad w_{\text{mean}} = 33.6 / (496) * (W-346) + 33.6 \quad (\text{A13})$$

985

$$986 \quad th_{\text{mean}} = 13.8 / (496) * (W-346) + 13.8 \quad (\text{A14})$$

987

988 It was assumed that the relative dispersion (SD/mean) of each variable was constant across rat  
989 weights, the SD value of each variable corresponding to rat weights of 200 and 250 g was  
990 computed from its measured values at 6 months to be proportional to the above computed  
991 mean value.

992 A series of values were generated as a set of 9 or 11 regularly spaced values of length,  
993 spanning the range ( $l_{\text{mean}} - \text{SD}$ ) to ( $l_{\text{mean}} + \text{SD}$ ), where SD is the standard deviation. Series of  
994 values for myocyte width and thickness were generated for each rat weights of 200 and 250 g  
995 with formulas (for the case of extrapolating to 200 g rat weight from 6 months rats), the  
996 indexes "200" and "6mo" mean 200 g and 6 months respectively:

997

$$998 \quad w = (1 - l_{\text{mean}}) * (\text{SD}_{w200}) / (\text{SD}_{w6\text{mo}}) + W_{\text{mean}} \quad (\text{A15})$$

999

$$1000 \quad th = (1 - l_{\text{mean}}) * (\text{SD}_{th200}) / (\text{SD}_{th6\text{mo}}) + th_{\text{mean}} \quad (\text{A16})$$

1001

### 1002 *6.3 Correction for the presence of caveolae*

1003 It has been measured in rabbit papillary muscle that caveolae augment plasmalemmal area by  
1004 21-32%, assuming two or three caveolae per neck, respectively (Levin and Page, 1980). This  
1005 is true for peripheral and TATS membranes. Page (1978) showed that in rabbit papillary  
1006 muscle the caveolar plasma membrane contributed 14-21% to the total plasmalemma with no  
1007 significant difference between the tubular system and external sarcolemma. Rat myocytes  
1008 have more caveolae necks than rabbit and extended branched chains of caveolae were  
1009 observed in rats (Severs et al., 1982). Thus 21% is likely to be in the lower range of realistic  
1010 values for the rat. The correction factor for caveolae is thus 1.21.

1011

### 1012 *6.4 Computing the increase in membrane area due to membrane infolding*

1013 Peripheral membrane presents sizeable infolding that is readily visible in scanning EM  
1014 microscopy (Nag et al., 1977; Nag and Zak, 1979) and was termed Z-folds (Severs et al.,  
1015 1985). Scanning ion conductance microscopy (SICM) has been used to confirm and further  
1016 characterize this infolding in freshly dissociated rat ventricular myocytes that was defined as  
1017 'Z-grooves' (Gorelik et al., 2006).



1018 Assuming that the profile of the transverse section of the peripheral membrane through Z-  
1019 grooves profile is a succession of half ellipses (Gorelik et al., 2006) with a and b being the  
1020 short and long radii, then the ratio of the ellipsoid profile to the linear one is:

1021  
1022 
$$\text{profile length} = \pi * \text{sqrt} [ 2 * (a^2 + b^2) - (a-b)^2 / 2 ] / 2 = 2.0563 \mu\text{m}, \quad (\text{A17})$$

1023  
1024 where  $a=0.35 \mu\text{m}$  and  $b=0.9 \mu\text{m}$ . The flat profile length is  $1.8 \mu\text{m}$ , thus the increase in profile  
1025 length is by a factor

1026  $2.0563 / 1.8 = 1.1424$  at the level of Z-grooves. Thus, the overall factor taking into account  
1027 the Z-groove factor is:

1028  
1029 
$$((1-Z) + Z * 1.1424) = 1.12. \quad (\text{A18})$$

1030  
1031 This factor should only apply to peripheral membrane excluding the intercalated disks (see  
1032 below).

1033 The membrane area due to infolding and to caveolae is included into the measured myocyte  
1034 capacitance. It is not included when peripheral membrane area is computed from myocyte  
1035 shape, or when tubular membrane area is estimated from the smoothed profile of TATS in  
1036 electron microscopy or confocal microscopy. It was thus needed to correct morphological  
1037 estimates of the peripheral membrane area by a factor of  $1.12 + 0.21$ , i.e. 1.33 that corrected  
1038 altogether for caveolae and infolding and that of TATS membrane area for caveolae only, i.e.:  
1039 by a factor of 1.21.

1040

#### 1041 *6.5 Effect of membrane infolding and caveolae on measured myocyte volume*

1042 Neglecting infolding and caveolae might misestimate myocyte volume but this ought not to  
1043 be significant since caveolae have a very large area to volume ratio and since alternating gain  
1044 and loss of small volumes across the mid-profile through membrane infolding likely cancelled  
1045 each other.

1046

#### 1047 *6.6 Intercalated disk area*

1048 There is considerable infolding of myocyte membrane at the level of the intercalated disk,  
1049 which increases membrane area by 2.3 fold from a flat plane through the intercalated disk  
1050 (Hoyt et al., 1989). The area of membrane at the myocyte endings (i.e.: twice the cross section

1051 area) represents about 6% of the total peripheral membrane area. No correction for caveolae  
1052 was applied to this area.

1053 Whenever the peripheral membrane area measurement has been reported as a whole, we  
1054 applied the above assumption. The overall correcting factor for the increase in peripheral  
1055 membrane area due to caveolae, membrane infolding and intercalated disk indentations is  
1056 then:  $0.06 * 2.3 + (1-0.06) * 1.33 = 1.39$ . The correction factor for TATS membrane area  
1057 includes caveolae only and amounts to 1.21.

1058

### 1059 *6.7 Specific membrane capacitance*

1060 Gentet et al. (2000) found a specific capacitance of  $0.9 \mu\text{F}/\text{cm}^2$  in several types of neurons.  
1061 This is not influenced by the amount of exogenously expressed protein. Likewise, Gilai  
1062 (1976) found values of  $0.90$  and  $0.91 \mu\text{F}/\text{cm}^2$  respectively for surface and for tubular  
1063 membrane of skeletal muscle fibres. Consequently, the true specific capacitance ought to be  
1064 lower than the canonical value of  $1 \mu\text{F}/\text{cm}^2$ . Thus, a value of  $0.9 \mu\text{F}/\text{cm}^2$  may be regarded as  
1065 an upper limit of the real specific capacitance. This value was used to translate capacitance  
1066 into membrane area. The canonical value of  $1 \mu\text{F}/\text{cm}^2$  was also used to allow comparisons  
1067 with the literature that mostly used this value.

1068

### 1069 *6.8 Corrections to myocyte volume: rendering factor*

1070 Whenever volumes computed from the idealized shape of myocytes ought to be compared to  
1071 3D-rendered volumes estimated from confocal images of real myocytes, they were corrected  
1072 for the discrepancy of the rendered volume to the geometrical computation of myocyte  
1073 volume as was estimated by Satoh et al. (1996).

1074 When mean values for myocyte length, width and thickness in table 2 of Satoh et al. (1996)  
1075 are used to compute the volume of a rod-shaped myocyte with elliptic cross section, volumes  
1076 of  $41818 \mu\text{m}^3$  and  $50717 \mu\text{m}^3$  are found for average myocytes of 3 months old rats and 6  
1077 months old rats respectively. These volumes translate to 41.8 and 50.7 pL respectively,  
1078 whereas mean rendered volumes in Satoh et al. (1996) were 30.9 and 36.8 pL respectively.  
1079 Thus the correction factor is respectively 0.74 and 0.73. This indicates that the correction  
1080 factor did not differ significantly between the two ages. However, they noted that the shape of  
1081 cardiac ventricular myocytes was more indented in older animals. Therefore, the correction  
1082 factor was assumed to be higher for 250 g (0.80) and 200 g rats (0.90). We used these values  
1083 to translate computed volumes into rendered volumes at different ages.

1084

## 1085 6.9 *Peripheral area to volume ratio*

1086 Peripheral myocyte area was computed as corresponding to a rod-shaped myocyte with  
1087 ellipsoidal cross section (Sorenson et al., 1985; Boyett et al., 1991). However, it was  
1088 estimated by Satoh et al. (1996) that the volume estimated from 3D volume rendering was  
1089 29% smaller than that of a rod-shaped myocyte with ellipsoidal cross-section, which they  
1090 attributed to uneven width of the myocyte along its long axis. In such a case, the projected  
1091 area of the real myocyte would also be about 29% smaller than the projection area of the  
1092 idealized rod shaped myocyte evaluated as the product of length by width. It is supported by  
1093 the finding of Satoh et al. that rendered volume is proportional to this product (length by  
1094 depth) (their figure 4A). This is approximately the case within our synthetic datasets (Fig.  
1095 1B). Therefore, myocyte peripheral area would be overestimated by the same fraction as  
1096 myocyte volume in the present computations, so that the peripheral area to volume ratio  
1097 computed for a rod with elliptic cross section should be equivalent to the area to volume ratio  
1098 of the real myocyte.

1099

## 1100 6.10 *Capacitance to volume ratio at low weights*

1101 The smallest myocyte in a 200 g rat in our synthetic data series (ellipsoidal section-rod shaped  
1102 myocyte with length 80  $\mu\text{m}$ , width 14  $\mu\text{m}$ , thickness 7.2  $\mu\text{m}$ ) has an uncorrected computed  
1103 peripheral area to volume ratio of  $0.45 \mu\text{m}^2/\mu\text{m}^3$ , which translates to 4.5 pF/pL assuming 1  
1104  $\mu\text{F}/\text{cm}^2$  as specific capacitance (or 4.05 pF/pL assuming  $0.9 \mu\text{F}/\text{cm}^2$ ). If now applying  
1105 corrections with an infolding factor of 1.12 and caveolae factor of 1.21, this ratio is  $0.644$   
1106  $\mu\text{m}^2/\mu\text{m}^3$ , which translates to 6.44 pF/pL (or 5.8 pF/pL with  $0.9 \mu\text{F}/\text{cm}^2$ ). Thus, within the  
1107 assumption that the linear relation of total membrane area to myocyte volume ratio also  
1108 applies to myocytes of animals younger than those studied by Satoh et al. (1996), the total  
1109 membrane area to volume ratio is likely to reach a minimal value that is determined by the  
1110 maximal peripheral membrane area to volume ratio attained for the smallest myocytes.  
1111 Therefore, it was assumed that the constant area to volume ratio for 200 and 250 g rats was  
1112 the same as for 3 months rats, i.e.  $0.676 \mu\text{m}^2/\mu\text{m}^3$ , which translates to 6.76 pF/pL with 1  
1113  $\mu\text{F}/\text{cm}^2$  or 6.08 pF/pL with  $0.9 \mu\text{F}/\text{cm}^2$ .

1114

## 1115 6.11 *Converting capacitance to volume ratio into area to volume ratio*

1116 The conversion of the measured total myocyte capacitance to volume ratio ( $k_c$  in pF/pL) into  
1117 area to volume ratio ( $k_a$  in  $\mu\text{m}^2/\mu\text{m}^3$ ), assuming that the peripheral and TATS membranes  
1118 have the same specific capacitance ( $sc$  in  $\mu\text{F}/\text{cm}^2$ ) is done using:

1119

$$1120 \quad \mathbf{k}_a = \mathbf{k}_c / \mathbf{s}_c * 10^{-1} \quad (\mu\text{m}^2/\mu\text{m}^3) \quad (\text{A19})$$

1121

### 1122 6.12 *Fraction of membrane in the TATS*

1123 If  $\mathbf{S}_{\text{surf}}/\mathbf{V}_{\text{myo}}$  is the computed peripheral membrane area to myocyte volume ratio, then the

1124 TATS membrane area to myocyte volume ratio is given by:

1125

$$1126 \quad \mathbf{S}_{\text{tt}}/\mathbf{V}_{\text{myo}} = \mathbf{S}_{\text{tot}}/\mathbf{V}_{\text{myo}} - \mathbf{S}_{\text{surf}}/\mathbf{V}_{\text{myo}} \quad (\mu\text{m}^2/\mu\text{m}^3) \quad (\text{A20})$$

1127

1128 This expresses the hypothesis that TATS morphogenesis obeys the constraint of maintaining a

1129 constant membrane area to volume ratio.

1130

1131 The fraction of myocyte membrane located in the TATS is computed as:

1132

$$1133 \quad \mathbf{S}_{\text{tt}}/\mathbf{S}_{\text{tot}} = \mathbf{S}_{\text{tt}}/\mathbf{V}_{\text{myo}} / (\mathbf{S}_{\text{tot}}/\mathbf{V}_{\text{myo}}) \quad (\text{dimensionless}) \quad (\text{A21})$$

1134

1135 **Captions to figures**

1136

1137

1138 **Figure 1:** Properties of the synthetic datasets representing ventricular myocytes in 6 months  
1139 (~500 g, circles), 3 months (~350 g, squares) and younger rats (250 g, triangles and 200 g,  
1140 diamonds). The symbols are connected by straight-line segments. **A:** Ratios of the peripheral  
1141 area to myocyte volume  $S_{\text{surf}}/V_{\text{myo}}$  computed for the four series of synthetic data sets were  
1142 plotted versus myocyte volume. **B:** The computed myocyte volumes were plotted versus the  
1143 projected areas. **C:** The total myocyte capacitance values were plotted versus myocyte  
1144 volume.

1145

1146

1147 **Figure 2:** Fraction of membrane area located in the TATS at different ages, plotted versus  
1148 myocyte volume. Symbols of each synthetic data set are as in Fig. 1. The four graphs (open  
1149 symbols plus line) are identical in panels **A** and **B**; they show the output of our simulations.  
1150 Additional grey-filled symbols show data derived by stereological measurements from  
1151 electron- or confocal-microscopy images (see Tab. 1 where the plotted data have been  
1152 overshadowed in grey colour). The shape of the symbols is the same as the weight class of the  
1153 corresponding rats. The numbers near the grey-filled and largest symbols refer to each study  
1154 as indicated in the leftmost column of Tab. 1. In **A**, these symbols show data from Sprague-  
1155 Dawley rats. The two largest symbols (labelled 9 and 10) refer to the TATS membrane  
1156 fractions computed from the data of Satoh et al. (1996). In **B**, the filled symbols report  
1157 measurements from Wistar rats. The two diamonds connected with a line labelled (2) are from  
1158 data related to Pager (1971) in Tab. 1.

1159

1160

1161 **Figure 3:** Values of the TATS membrane fraction as evaluated from morphological studies  
1162 (filled symbols, Tab. 1) or detubulation studies (open symbols, Tab. 2) in Sprague-Dawley  
1163 rats (lozenges), Wistar rats (circles) or rats of unspecified strain (triangles). Values the TATS  
1164 membrane fraction ( $S_{\text{tt}}/S_{\text{tot}}$ ) from Tab. 1 were expressed in %, instead of fraction, to allow  
1165 comparison with data from Tab.2. In **A**, all values were plotted for each of the two methods.  
1166 The three series of data were offset horizontally for clarity. A further variable horizontal  
1167 offset was applied to the symbols within a given series, for clarity. In **B**, values were plotted  
1168 versus weight. When not available, weight was defaulted to zero.

1169  
1170  
1171  
1172  
1173  
1174  
1175  
1176  
1177  
1178  
1179  
1180  
1181  
1182  
1183  
1184  
1185  
1186  
1187  
1188  
1189  
1190

**Figure 4:** Relationship of the membrane fraction in TATS  $S_{tt}/S_{tot}$  (expressed in %) with body weight, as determined from morphological studies in Sprague-Dawley rat myocardium (Tab. 1). Open squares report the mean TATS membrane fraction versus mean weight values. A uniform relative standard deviation of 0.2 was assumed for both body weight and TATS membrane fraction measurements (respectively  $s_{xi}$  and  $s_{yi}$ ) and are reported as error bars. Weighting of the fit included both errors in the form:  $w_i = 1/((B*s_{xi})^2 + s_{yi}^2)$ . The solid line equation was  $y = A + B*x$  with  $A = -10.4 \pm 17.5 \%$  and  $B = 0.167 \pm 0.065 \%/g$ . The dashed lines show the upper and lower 95% confidence limits. The calculation of Pearson's correlation coefficient R was omitted because it neglects any error associated with the mean values.

**Figure 5:** Weights and ages of Wistar rats were collected from the detailed study of Nakamura et al. (1986) and their relationship was plotted (filled squares), with error bars reporting the span of weights and/or age, when present. The regression line indicates proportionality with a slope of about 30 g / week. Open circles show the data for Wistar rats in Tab. 1 and 2. Open triangles report the data for Sprague-Dawley rats. When not reported, a putative 10% dispersion of the weight was associated with open symbols.

		Strain	Age (weeks) /sex	Weight g	Method	C <sub>m</sub> / n	V <sub>tt</sub> /V <sub>myo</sub>	S <sub>surf</sub> /V <sub>myo</sub>	S <sub>tot</sub> /V <sub>myo</sub>	S <sub>tt</sub> /V <sub>myo</sub>	S <sub>tt</sub> /S <sub>tot</sub>	3D-Rendering factor
						pF	μm <sup>3</sup> /μm <sup>3</sup>	μm <sup>2</sup> /μm <sup>3</sup>	μm <sup>2</sup> /μm <sup>3</sup>	μm <sup>2</sup> /μm <sup>3</sup>		
1	Page et al., (1971)	Sprague-Dawley	na/F	200	Stereology EM	na	<b>0.012</b>	<b>0.27</b> <i>0.33<sup>c</sup></i>	<b>0.34</b> <i>0.41<sup>c</sup></i>	<i>0.07</i> <i>0.0847<sup>c</sup></i>	<i>0.207</i> <b>0.207</b>	
2	Pager, (1971)	Wistar	Adult / na	200	Stereology EM	na	<b>0.0106</b>		<i>0.44*</i> <i>0.49**</i> <i>0.76*</i> <i>0.84**</i>	<b>0.25</b> <b>0.30<sup>c</sup></b> <b>0.30<sup>c</sup></b> <b>0.30<sup>c</sup></b>	<i>0.57</i> <b>0.61</b> <i>0.39</i> <b>0.35</b>	
3	Page and McCallister, (1973a)	Normal rat	na / na	200	Stereology EM	na	<b>0.01</b>	<b>0.3</b> <i>0.36<sup>c</sup></i>	<b>0.39</b> <i>0.47<sup>c</sup></i>	<i>0.09</i> <i>0.109<sup>c</sup></i>	<i>0.23</i> <b>0.23</b>	
4	Page, (1978) <sup>1</sup>	Rat	na / na	na	Stereology EM	na					<b>0.33</b>	
5	Stewart and Page, (1978)	Sprague-Dawley	na / F	222	Stereology EM	na	0.004	<b>0.3</b>	<b>0.43</b>	<b>0.13</b>	<b>0.30</b>	
6	Stewart and Page, (1978)	Sprague-Dawley	na / F	300	Stereology EM	na	0.008	<b>0.3</b>	<b>0.47</b>	<b>0.16</b>	<b>0.34</b>	
7	Page and Surdyk-Droske, (1979)	Sprague-Dawley	na / F	200-260	Stereology EM	na	na	<b>0.307</b> <i>0.371<sup>c</sup></i>	<i>0.457</i> <i>0.553<sup>c</sup></i>	<b>0.145</b> <i>0.175<sup>c</sup></i>	<i>0.32</i> <b>0.32</b>	
	Nakamura et al., (1986)	Wistar	7/FM	200	Stereology EM	na	<b>0.0075</b>		<i>0.676*</i>	<b>0.30</b> <i>0.363<sup>c</sup></i>	<i>0.44</i> <b>0.48</b>	
9	Satoh et al., (1996) 3 months rats	Sprague-Dawley	3 months / M	346 (330-378)	Confocal 3D	207±8.3 / 14	na	<i>0.308<sup>cf</sup></i>	<b>0.676*</b> <b>0.75**</b>	<i>0.368*</i> <i>0.442**</i>	<i>0.544</i> <b>0.589</b>	<i>0.74</i>
10	Satoh et al., (1996) 6 months rats	Sprague-Dawley	6 months / M	496 (480-516)	Confocal 3D	324±14 / 14	na	<i>0.295<sup>cf</sup></i>	<b>0.888*</b> <b>0.99**</b>	<i>0.593*</i> <i>0.695**</i>	<i>0.668</i> <b>0.702</b>	<i>0.73</i>
11	Soeller and Cannell, (1999)	Wistar	na / na	250	Confocal 3D	na	<b>0.036</b>		<b>0.676*</b> <b>0.75**</b> <i>0.843*</i> <i>0.94**</i> <i>0.76*</i> <i>0.84**</i>	<b>0.44</b> <b>0.44</b> <b>0.44</b> <b>0.44</b> <b>0.44</b> <b>0.44</b>	<i>0.65</i> <i>0.59</i> <i>0.52</i> <b>0.47</b> <i>0.58</i> <b>0.52</b>	<i>0.71</i>
12	Despa et al., (2003)	Sprague-Dawley	11 <sup>4</sup> / M	~300	Confocal 3D	156±7 / 24	na	<i>0.373<sup>cf</sup></i>	<b>0.51*</b> <b>0.57**</b>		<i>0.27</i> <b>0.36</b>	
13	Swift et al., (2006)	Wistar	na / M	300	Confocal 3D	199±9 / 9	na	<i>0.361<sup>cf</sup></i>	<b>0.843*</b> <b>0.94**</b>		<i>0.57</i> <b>0.62</b>	
14	Gorelik et al., (2006)	Sprague-Dawley	Adult / M	490	Confocal 3D	na	na	na			<b>0.728</b> <b>0.432<sup>3</sup></b>	

Table 1: Available quantitative morphological estimates describing the amount of TATS membrane area in rat myocytes.

1194 In bold: values measured by the authors. In italics: values computed from their data (see section 3.2). na: not available. \* and \*\*: computed from  
1195 authors' data, assuming a specific capacitance of \*  $1 \mu\text{F}/\text{cm}^2$  or \*\*  $0.9 \mu\text{F}/\text{cm}^2$ . <sup>1</sup> Quoted by (Yao et al., 1997) and (Satoh et al., 1996). <sup>2</sup> This is  
1196 the ratio of di-8-ANEPPS fluorescence in the TATS (whole confocal slice image minus peripheral membrane) to fluorescence from the whole  
1197 confocal slice. See section 3.2 for further discussion. <sup>3</sup> The same ratio in detubulated myocytes. <sup>4</sup> Age derived from breeder's data in Pasek et al.  
1198 2017. <sup>c</sup> Corrected for area of caveolae. <sup>f</sup> Corrected for membrane infolding.  
1199



Ref	Animal/strain	Weight (g) / Age (week)	C <sub>m</sub> eval. method	C <sub>m</sub> control (pF) / n	C <sub>m</sub> detubul. (pF) / n	% C <sub>m</sub> lost / f <sub>tres</sub>	C <sub>m</sub> /V <sub>myo</sub> (pF/pL)	% C <sub>m</sub> lost corr.	V <sub>myo</sub> (pL)
Kawai et al., (1999)	Adult female Wistar	na	na	199.4 ± 19 / 13	146.7 ± 6.4 / 13	26.6		32.2	
Komukai et al., (2002)	Adult male Wistar	250	na	200 ± 7 / 37	160 ± 8 / 23	20.0		24.4	
Yang et al., (2002)	Adult male Wistar	~250 / 7*	na	193 ± 41 / 25	143 ± 34 / 25	25.9 / 0.08		31.6	
Despa et al., (2003)	Male Sprague-Dawley	~300 / 11*	na	156 ± 7 / 24	106 ± 5 / 19	32.1 / 0.08		39.1	
Thomas et al., (2003)	Male Wistar	~300 / 9*	Integration	204 ± 11 / 23	150 ± 7 / 13	26.5 / 0		32.3	
Brette et al., (2004a)	Male Wistar	na	na	193 ± 22 / 22	137 ± 34 / 22	29.0		35.4	
Brette et al., (2004b)	Male Wistar	na	Integration	178 ± 11 / 11	132 ± 3 / 10	25.8		31.5	
Duclohier, (2005)	Adult male Sprague Dawley <sup>1</sup>	na	na	135 ± 7 / 13	105 ± 9 / na	22.2		27.1	
Brette et al., (2006)	Male Wistar	250-300	Integration	186 ± 11 / 14	133 ± 8 / 13	28.5		34.7	
Swift et al., (2006)	Male Wistar	~300	Integration	199 ± 9 / 9	140 ± 14 / 7	29.6 / 0.08 <sup>6</sup>	8.4	36.2	23.6
Brette and Orchard, (2006a)	Male Wistar	na	na	156 ± 9 / 14	115 ± 5 / 17	26.3		32.1	
Brette and Orchard, (2006b)	Male Wistar	na	na	174 ± 9 / 24	120 ± 5 / 25	31.0		37.8	
Despa and Bers, (2007)	Rat	na	na	164 ± 6 / 12	120 ± 8 / 9	27.0		32.7	
Swift et al. (2007)	Male Wistar	~300 / ~10	Integration	235 ± 7.8 / 11	178 ± 7 / 11	24.3 / 0.08 <sup>6</sup>	7.6	29.6	30.8
Swift et al. (2008)	Male Wistar	~300 / ~10	Integration	237 ± 15 / 11	181 ± 6 / 11	23.6 / 0.08 <sup>6</sup>		28.8	
Chase et al., (2010)	Male Wistar	na	na	207.3 ± 11.0 / 13	144.7 ± 5.5 / 18	30.2		36.8	
Garciarena et al., (2013) <sup>5</sup>	Adult male Sprague Dawley	300 / 11*	Integration	236 ± 26 / 9	139 ± 14 / 8	41.0	14.4	50.1	16.4
Bryant et al., (2014)	Adult male Wistar	250-300	na	283 ± 22 / 11	167 ± 11 / 11	41 /		50.0	
Bryant et al., (2015)	Adult male Wistar <sup>2</sup>	~460 / ~25	na	260 ± 9 / 37	178 ± 9 / 28	31.5		38.5	
Gadeberg et al. (2016)	Male Wistar	~460 / ~25	na	240.2 ± 21 / 12	206.2 ± 11 / 9 <sup>7</sup>	14.2 / 0.16		--	
Bourcier et al., (2019)	Male Wistar	250-300	na	184.2 ± 10.8 / 21 <sup>3</sup>	105.2 ± 6.4 / 21 <sup>3</sup>	40.6 <sup>4</sup> (43.0)		52.3	
Mean values				201 ± 8	143 ± 6	28.5 ± 1.5		35.7 ± 1.7	

1201

1202 Table 2: Values of changes in membrane capacitance upon formamide detubulation of adult rat ventricular myocytes. Values are mean ± sem  
1203 with the number of myocytes n.

1204 <sup>1</sup> – Isolated myocytes obtained from Harding SE's lab, who worked with Adult male Sprague Dawley rats (Lewis et al., 2004).

1205 <sup>2</sup> – 18 weeks after sham coronary artery ligation operation.

1206 <sup>3</sup> – The sem was computed from original SD.

1207 <sup>4</sup> – original value at 43 % was corrected for 6% incomplete detubulation to match conditions of formamide detubulation in other studies.

1208 <sup>5</sup> – data was read from their figure 2B.

1209 <sup>6</sup> – Detubulation incomplete as discussed by authors.

1210 <sup>7</sup> – Detubulated data in control rat as indicated in Pasek et al., (2017).

1211 \* Age derived from from the growth chart at <http://www.criver.com/> by Pasek et al., (2017).

1212

Figure 1

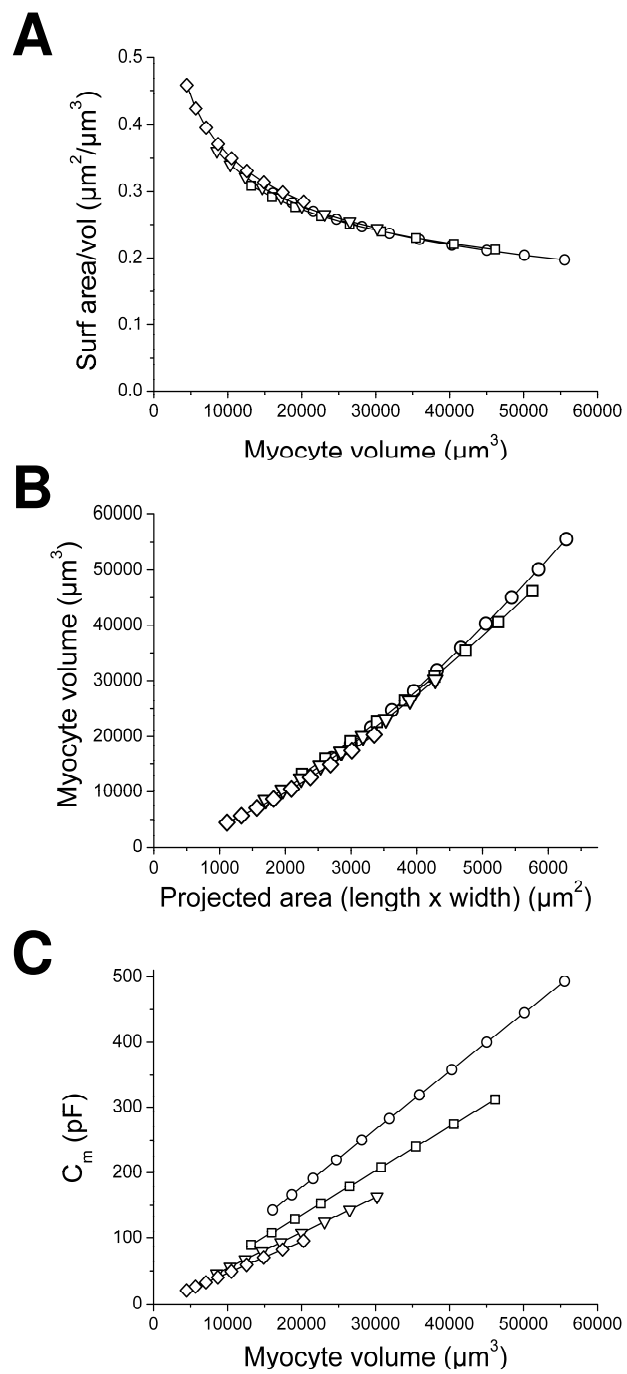


Figure 2

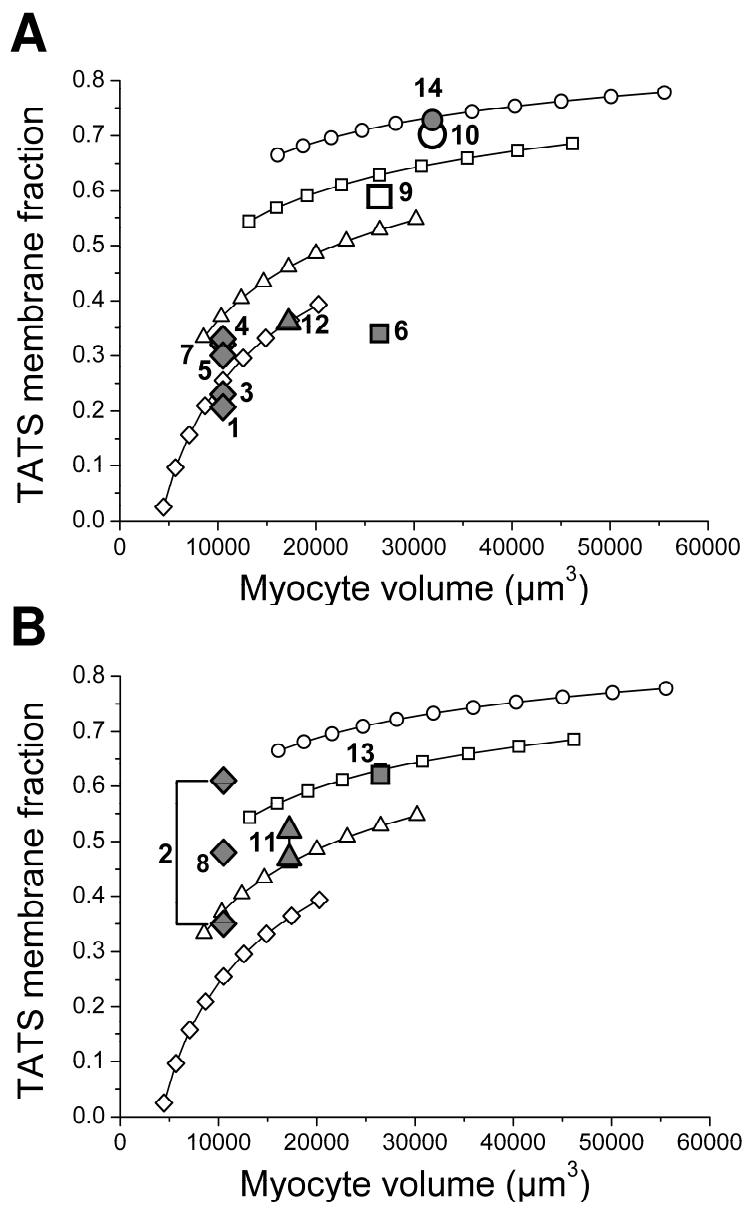


Figure 3

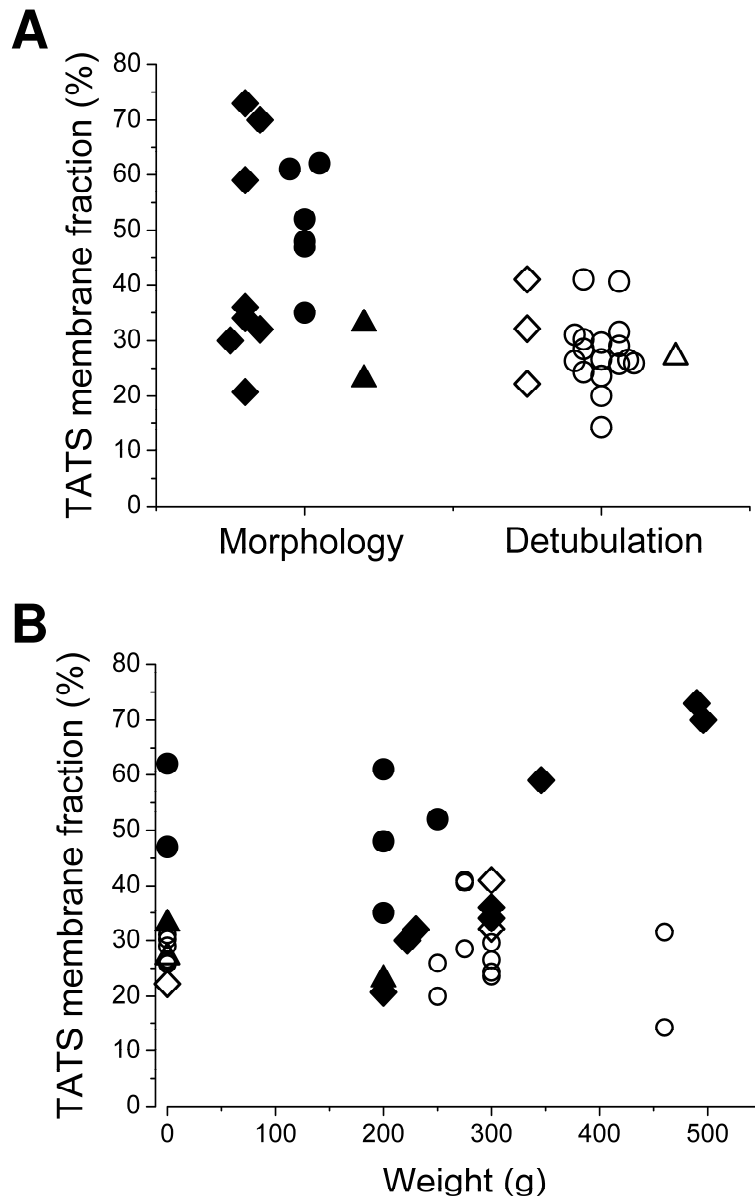


Figure 4

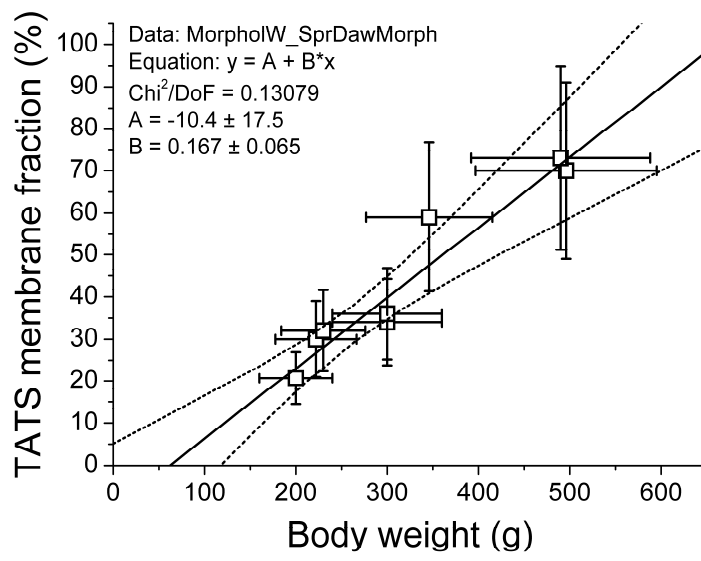


Figure 5

